#230

NOAA TM ERL SEL-42

RECORD SET

NOAA Technical Memorandum ERL SEL-42

U.S. DEPARTMENT OF COMMERCE
NATIONAL OCEANIC AND ATMOSPHERIC ADMINISTRATION
Environmental Research Laboratories

The SMS/GOES
Space Environment Monitor Subsystem

R. N. GRUBB

Space
Environment
Laboratory
BOULDER,
COLORADO
December 1975

NOAA Technical Memorandum ERL SEL-42

THE SMS/GOES
SPACE ENVIRONMENT MONITOR SUBSYSTEM

R. N. Grubb

Space Environment Laboratory
Boulder, Colorado
December 1975

UNITED STATES
DEPARTMENT OF COMMERCE
Rogers C.B. Morton, Secretary

NATIONAL OCEANIC AND
ATMOSPHERIC ADMINISTRATION
Robert M. White, Administrator

Environmental Research
Laboratories
Wilmot N. Hess, Director

TABLE OF CONTENTS

LIST OF FIGURES

TABLE OF CONTENTS (CONT.)

LIST OF TABLES

THE SMS/GOES SPACE ENVIRONMENT MONITOR SUBSYSTEM

R. N. Grubb

The Space Environment Monitor Subsystem, which is incorporated in the satellites SMS-1, SMS-2, and GOES-A, is described. The subsystem contains an energetic charged particle sensor, a magnetometer, and a soft solar x-ray detector and is intended for real time use by the Space Environment Services Center and to provide a long term scientific data base.

Key Words: Geostationary satellite, magnetic field, monitoring, particles, x rays

1. INTRODUCTION

The Synchronous Meteorological Satellite (SMS) series is being built by the National Aeronautics and Space Administration (NASA), Goddard Space Flight Center (GSFC), to meet the operational requirements of the National Oceanic and Atmospheric Administration (NOAA). Two SMS vehicles have been built to be followed by at least 3 similar satellites procurred with NOAA funds to be known as Geostationary Operational Environmental Satellites (GOES). The principal sensor system is a 20 inch diameter visible and infrared radiometer system (VISSR) for high resolution spin scan imaging of the earth. The communication subsystem provides for transmission of the VISSR data to the primary Command and Data Acquisition Station at Wallops Island, Virginia, as well as for retransmission of time stretched VISSR data, data collection and relay from remote sensor platforms, and standard telemetry and command functions.

The Space Environment Monitor (SEM) subsystem is designed to provide data for use in real time, and for subsequent analysis and dissemination, by the Space Environment Laboratory (SEL), a component of the Environmental Research Laboratories of NOAA, in Boulder, Colorado. This Laboratory is the national and international focal point for current information concerning the solar terrestrial environment and supplies this information as a continuing service to a wide variety of users. Dissemination is made by a number of means ranging from outside interrogation of real time computer data base, daily forecasts and advisory messages, weekly and monthly publication of data, to the deposit of historical data with the Environmental Data Service, and other data centers.

The SEM has been provided as part of the main spacecraft procurement by the contractor, Aeronutronic Ford Corporation*, to meet performance specifications set by SEL. A large number of people have contributed to the final design both within Aeronutronic Ford and their subcontractors and within the GSFC SMS project group and SEL staff. Detailed acknowledgment would be impossible, but a list of the major individuals involved is given in

*Formerly Philco-Ford Corporation

the acknowledgment. The objective of this report is to bring together in convenient form all the information on the SEM pertinent to the use of the data and includes design analysis only to the extent necessary to understand the basic function of the sensors. Much of the graphic material is abstracted from contractor publications.

As the sensors are operational monitoring instruments, no formal principal investigator structure exists. Overall project scientist control for NOAA rests with Dr. D. J. Williams, Director of the Space Environment Laboratory.

The SEM subsystem comprises three separate sensor systems, each interfaced to the vehicle PCM telemetry encoder. The sensors are an Energetic Particle Sensor (EPS), a Magnetometer, and a Solar X-Ray Instrument.

The energetic particle monitoring system measures that portion of the particle environment at 6.6 earth radii which has effects of practical significance to man's activities. High energy solar protons and alpha particles (helium nuclei) are accelerated during some energetic solar flares, and large fluxes of these particles can reach the immediate vicinity of the earth. The path followed by the solar particles is controlled by the interplanetary solar magnetic field and the time of arrival and spectrum of the arriving particles reflects the original spectrum and the dispersion due to the travel time. Particles with energies greater than about 10 MeV can constitute a significant radiation hazard to manned space flight operations, and those with energies greater than about 160 MeV can create a hazard to passengers and crew of aircraft operating at high latitudes. Lower energy protons increase the D-region ionization in the high latitude ionosphere, causing Polar Cap Absorption events which disrupt HF radio propagation relying on high latitude reflection points.

The magnetometer measures the magnitude and direction of the magnetic field. Under normal conditions, the geostationary orbit of SMS takes the instrument through the earth's magnetic field close to the boundary at local noon and close to the geomagnetic tail region at local midnight. Important parameters of the shape of geomagnetic field, as distorted by the pressure of the solar wind, can be obtained from these measurements. The model of the field obtained can be used to predict charged particles dynamics and the behavior of the trapped radiation belts. Data from the magnetometer also provide early warning of geomagnetic substorms which, by dumping trapped particles in the radiation belts into the high latitude ionosphere, disrupt HF radio propagation. Under very disturbed conditions, shock fronts in the solar wind can compress the geomagnetic field bringing the boundary within the geostationary satellite orbit. These boundary crossings can be readily detected from the magnetometer data and the degree of field compression measured.

The solar x-ray instrument measures the flux of soft x rays from the sun in two bands 0.5-3 A and 1-8 A. This flux is indicative of the general level of solar activity and is often greatly enhanced during a solar flare.

It's probably the most sensitive technique for detecting the start of a flare.

There is also some evidence that flares are preceded by a gradual enhancement of soft x rays which may enable the forecasting of flares to be improved. The intensity and spectrum of x-ray emission during the flare are not particularly well correlated with the optical characteristics, and thus, the x-ray characteristic forms an important part of the description of the energetics of the event. The soft x-ray flux is responsible for immediate ionospheric effects within the sunlit hemisphere which create increased absorption of HF radio signals, often leading to complete loss of signals for the duration of the event.

Section 2, which follows, provides a summary of the salient characteristics of the satellite, the telemetry system, and the SEM for quick reference. The following sections provide more detailed information on the design of the individual sensors and the telemetry and data handling system.

2. SUMMARY OF THE SMS AND SEM SENSOR CHARACTERISTICS

2.1 SMS Satellite

The SMS (GOES) satellites are spin stabilized at 100 rpm nominal and are placed in a geostationary orbit. The spin axis is perpendicular to the plane of the orbit. The inclination should be held within ±1° for the first two years. The design lifetime of the spacecraft is five years. When two operational spacecraft are in orbit they will be placed at approximately 75° and 135°W.

Figure 2.1 shows the general appearance of the satellite. Figure 2.2 shows the positions of the SEM sensors. The magnetometer sensor is mounted on the tripod above the VHF antenna array. The EPS and solar x-ray sensors are mounted on the main equipment platform and look outwards radially through cutouts in the main solar all array panels. The main electrically despun S-band UHF electrically despun antenna arrays can be seen below the solar array. An onboard Attitude Determination And Control subsystem (ADAC) provides spin clock timing signals referenced to the vehicle sun line and the vehicle earth line, which are used by the solar x-ray sensor and the magnetometer, respectively, as well as for control of the VISSR and antenna subsystems.

Telemetry for the SEM and other vehicle parameters is provided by a 188 bps PCM system. The frame is 64 words long, and each word has 9 bits. Two subcommutation sequences are provided, one with a length of 32 frames and the second 64 frames. An additional special telemetry submultiplex sequence is generated within the SEM subsystem for the EPS data. Table 2.1 shows the allocations within the main frame for SEM data. The data are transmitted to the ground in biphase mark coding as PSK modulation on both the VHF telemetry transmitter and an S-band carrier which is inserted into the main S-band communications transponder system. The telemetry word numbering system used in this document runs from 1-64, 1 being the first frame synchronizing word.

2.2 The Energetic Particle Sensor

The energetic particle sensor consists of solid state detectors, each associated with preamplifier and pulse height discriminator system. The three higher energy detectors are 3 mm cubes located in a dome moderator assembly, and the two lower energy surface barrier detectors are mounted coaxially in a telescope assembly, both of which look out from the side of the spacecraft. The combination of detector shielding and pulse height discrimination and, in the case of the lower energy detectors, logical combination is utilized to provide a series of outputs in which the pulse rate represents the flux for a particular energy range and particle species. These pulses are routed to the Data Processor Unit (DPU), where they are sequentially gated into one or the other of two accumulators to provide a

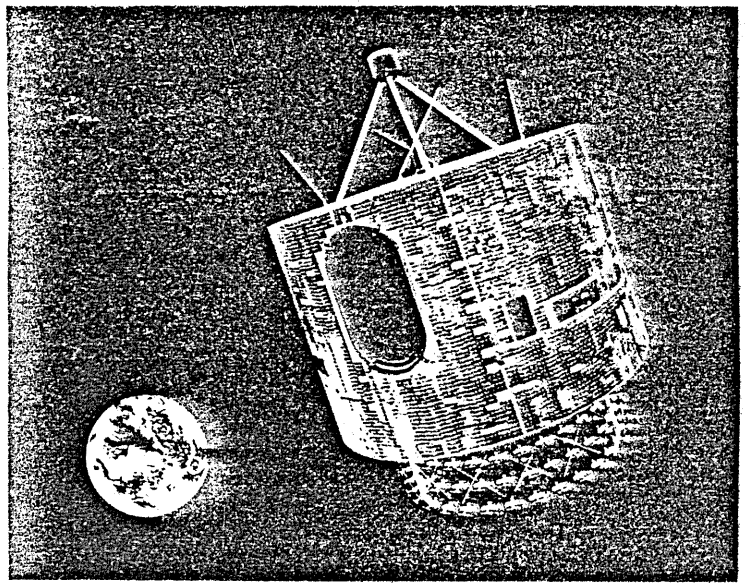

Figure 2.1 Synchronous Meteorological Satellite

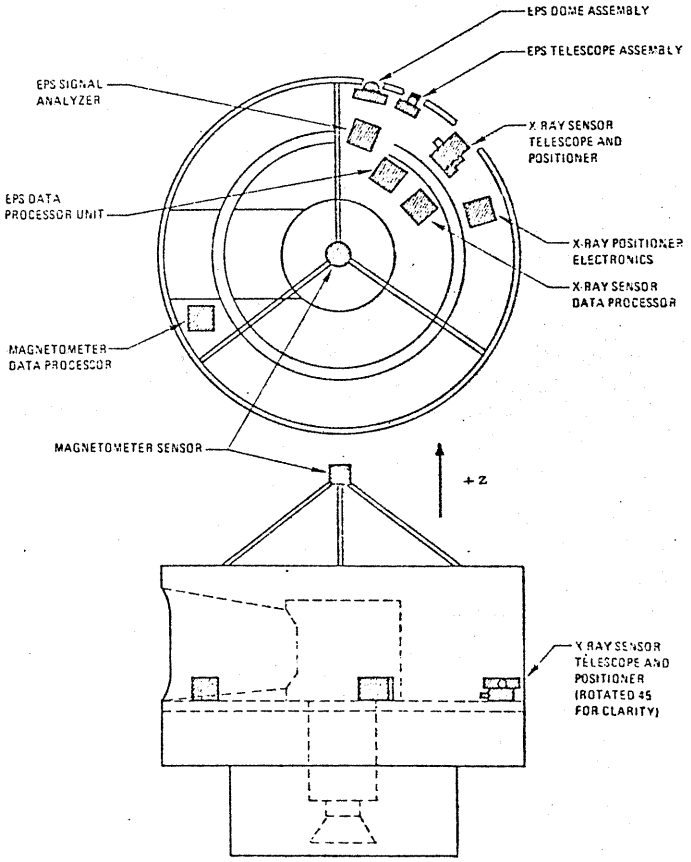

Figure 2.2 SEM Component Location on Spacecraft

Table 2.1 SEM Telemetry Format Usage

SYNC 11110110 1	SYNC 10100000 2	SUBMULT I/D 3	COMMAND VERIFY 4	D M_{4-12} 5	A M_1 6	A M_2 7	A M_3 8
9	10	11	12	13	14	D X_{5-9} 15	A X_2 16
17	A X_1 18	19	20	21	A M_1 22	A M_2 23	A M_3 24
25	26	27	A 64 SUBMULT M_{13-14} X_{11-12} E_{2-4} 28	29	30	$E_1 P_1$ 31	32
D 33	34	35	M_{4-12} 36	37	A M_1 38	A M_2 39	A M_3 40
41	42	43	44	45	46	47	48
49	50	51	X_{14} 52	D P_{6-7} a_{5-6} 53	A M_1 54	A M_2 55	A M_3 56
57	58	59	32 SUBMULT M_{15} X_{3-4} $X_{10} X_{13}$ E_5 60	61	62	D P_{2-5} a_{1-4} 63	A X_{15} 64

measure of particle flux. The accumulation times are chosen to provide suitable ranges of flux in conjunction with the use of quasi-logarithmic compression system within the accumulator which provides the range of approximately 4 decades within the telemetry word. An onboard calibration system exercises the electronic channels under ground command and verifies operation of the basic discriminators and accumulators. Table 2.2 gives the important parameters of each channel and the telemetry submultiplex sequence.

Table 2.2 Summary of EPS Outputs (Digital)

CHANNEL	ΔE (MeV)	GEOMETRIC FACTOR CM^2 STER	ACCUMULATION TIME (S)	TM WORD	SECONDS PER SAMPLE
P1	0.8-4.0	0.68 1.12	1.44	31	6.13
P2	4.0-6.0	0.23 .559	1.44	63	24.5
P3	6.0-10	0.23 1.0	1.44	63	24.5
P4	18 - 38	0.21	1.44	63	24.5
P5	40 - 500	0.21	1.44	63	24.5
P6	84 - 150	0.42	2.49	53	12.2
P7	150-500	0.42	2.49	53	12.2
α1	4.0-10	0.68	1.44	63	24.5
α2	10 - 16	0.23	1.44	63	24.5
α3	18 - 56	0.23	1.44	63	24.5
α4	71 - 150	0.21 30.5	1.44	63	24.5
α5	167-245	0.21 22.6	2.49	53	12.2
α6	340-392	0.42 91.7	2.49	53	12.2
E1	>2.0	0.21 1.572	1.44	31	6.13

Geo factor GOES 2 / GOES 3 / SMS-2

TELEMETRY SUBMULTIPLEX SEQUENCE
(START COINCIDES WITH START OF 64 CHANNEL SUBMULTIPLEXER)
WORD 31 (8 BITS) E1 P1 E1 —
63 (8 BITS) P2 P3 P4 P5 α1 α2 α3 α4 P2 —
53 (7 BITS) P6 P7 α5 α6 P6 ---

ANALOG CHANNEL	MEASURAND	RANGE	TM WORD	SECONDS PER SAMPLE
E2	DOME SENSOR TEMP	-70 TO +50°C	23 (9)	196.1
E3	TELESCOPE SENSOR TEMP	-10 TO +50°C	28 (57)	196.1
E4	DPU TEMP	-10 TO +50°C	28 (19)	196.1
E5	REFERENCE VOLTAGE	4.85 V	60 (9)	98.0

(count/sec)(Geo fac) = counts / cm^2 sec ster

Pass = PASWDSE
UN≠COWL
Family = SEL

AFIHMS

The geometric factors given are calculated from the geometry of the particular sensor. Individual instrument calibrations of counting efficiency and energy response have been made and will be used in determining the satellite ambient flux and spectrum from the data. Figure 2.3 shows the sensor system before integration with the spacecraft.

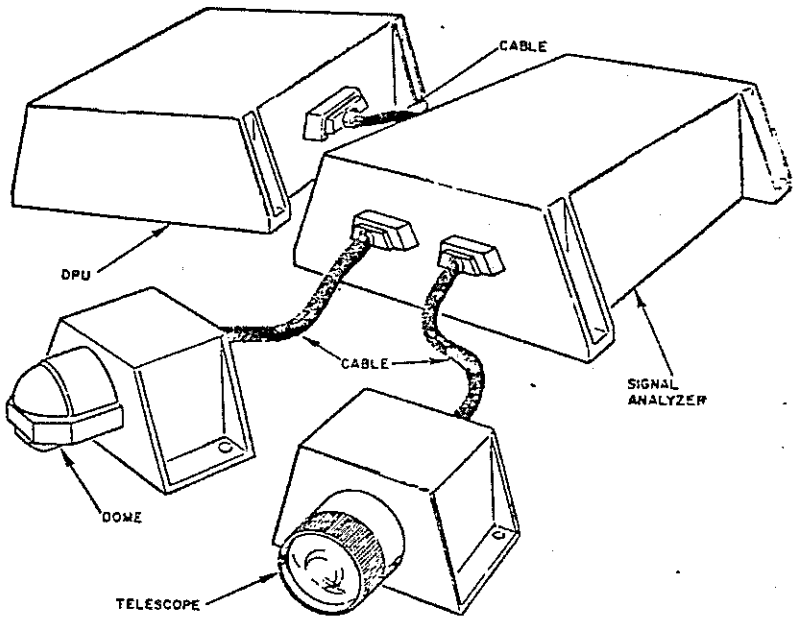

Figure 2.3 Energetic Particle Sensor System

2.3 Magnetometer

The magnetometer utilizes two flux gate sensors and the satellite spin to measure the magnitude and direction of the ambient magnetic field. The sensors are mounted together and supported by three short booms in a position above the VISSR mirror housing. The electronics for the sensors are mounted separately on the spacecraft equipment platform. One of the sensors, the "parallel" sensor, is mounted parallel to the vehicle spin axis and measures the vector component of the field in that direction. The second "transverse" sensor is mounted perpendicular to the spin axis and produces a sinusoidal output at the vehicle spin rate whose amplitude and phase represent the vector field within the vehicle equatorial plane. This signal is processed onboard to produce two quadrature component values with respect to a spatial reference supplied from the ADAC system. A combination of stepped offset and range selection enables the system to provide a basic 0.2 γ ($1\gamma = 10^{-5}$ gauss) sensitivity while accommodating

fields within the range of ±≃1200 γ for parallel components, ±400 γ for natural transverse components and ±1200 γ for spacecraft transverse fields. However, the absolute accuracy of the instrument will be limited in practice by the static and spin modulated vehicle fields which are expected to be both time varying and significant compared to the ambient field. Preflight calibration and post-flight experience should enable the resultant offsets to be subtracted with some degree of confidence. An onboard calibration system under ground command provides a calibration of basic instrument sensitivity and verifies operation of the offset and range changing system. Table 2.3 shows the major telemetry outputs, the scales, and telemetry allocations. Figure 2.4 shows the appearance of the sensor before integration.

Table 2.3 Magnetometer Outputs

Measurement	Type	Measurement Range	TM Word	Seconds/ Sample
M1 H Parallel	Analog	-50 to +50γ	6, 22, 38, 54	.766
M2 $H_t \cos \phi$		-50 to +50; -100 to +100; -200 to +200; and -400 to +400γ	7, 23, 39, 55	.766
M3 $H_t \sin \phi$		Same as M2	8, 24, 40, 56	.766
M4 H Parallel-offset	Digital	-1120 to +1400γ (83 steps of 40γ/step)		
M5 H Parallel-offset				
M6 H Parallel-offset			5,36 (8 bits)	1.53
M7 H Parallel-offset				
M8 H Parallel-offset				
M9 H Parallel-offset				
M10 H Transverse Range		Full Scale 50, 100, 200, or 400γ		
M11 H Transverse Range				
M12 Cal/Data		Cal/Data	5 (1 bit)	
M13 Sensor Temperature	Analog	-10 to +50°C	28 (63)	196.1
M14 Electronics Temperature	Analog	-10 to +50°C	28 (64)	196.1
M15 Reference Voltage	Analog	2.495 V	60 (5)	98.0

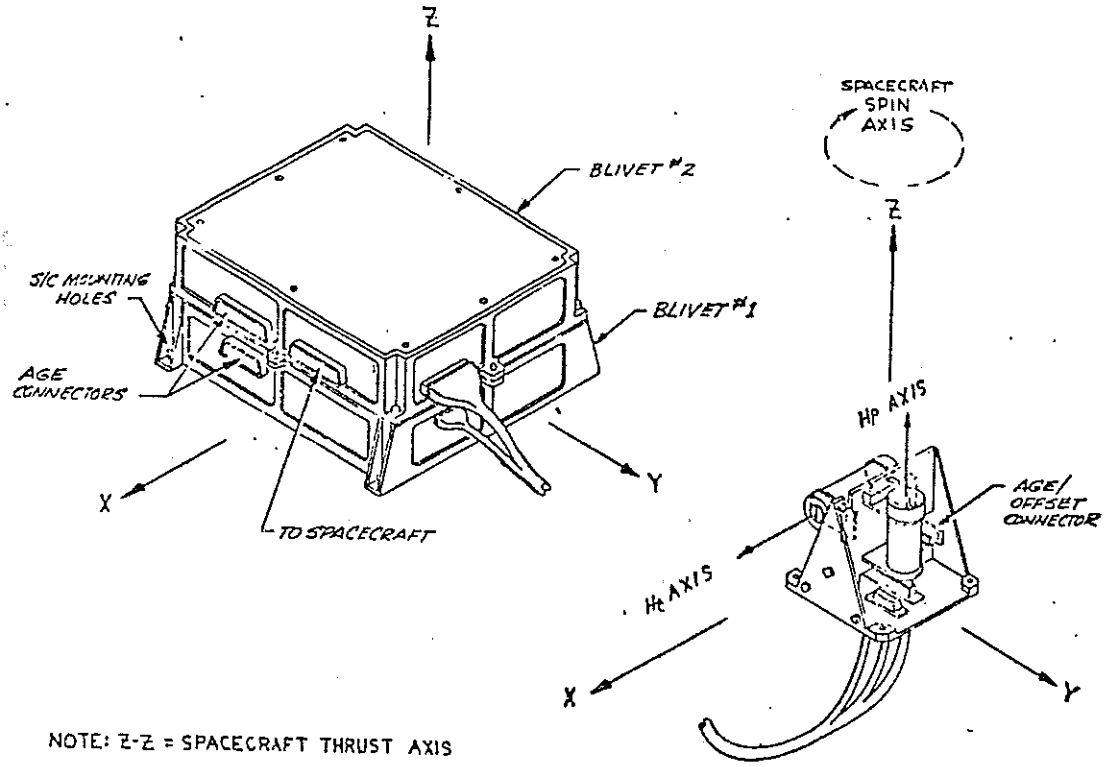

Figure 2.4 Magnetometer Sensor and Electronics Package

2.4 The Solar X-Ray Instrument

The basic Solar X-Ray Instrument consists of an x-ray sensor and an x-ray positioner (see figure 2.5). The solar x-ray sensor consists of two ion chambers in which the gas filling and window transmission characteristics are chosen to provide the desired x-ray response in the two bands 0.5-3 Å and 1-8 Å. These sensors are similar to those used for some years in the SOLRAD series of low orbiting satellites. In the absence of special precautions, however, the energetic electron environment would produce a much greater electrical output than the quiet sun.

The SMS ion chambers are mounted behind a common collimator which serves to reduce the access of electrons directly into the ion chamber window and, by means of a transverse magnetic field provided by a permanent magnet assembly, prevent electrons with energies less than ≃2 MeV from reaching the chamber. Electrons stopped by the collimator, ion chamber, and spacecraft structure produce a background of bremsstrahlung radiation. The overall background after collimation, although still large, can be removed from the measurement by a subtraction technique. First the

mean DC component is subtracted by current balancing feedback. Then the signal from the ion chamber, after amplification by an electrometer, is sampled twice during one satellite revolution, once during the time the sensor sees the sun, and once during the period immediately preceding. The two readings are effectively subtracted by the signal processing electronics to give the solar x-ray signal. Background readings of the mean ion chamber current and of the preamplifier output are provided separately as housekeeping information.

The collimator and ion chamber assembly is mounted on a single axis positioner drive which enables the look angle of the collimator to be varied by the ± 23.5° necessary to track the annual variation in angle between the satellite sun line and the satellite spin axis. The positioner is driven in 0.25° steps under ground command.

The data processing electronics cover a 4 decade range by means of automatic range selection. The analog output from each wavelength range is then converted by the spacecraft encoder into a 9 bit telemetry word. Indication of range in use and calibration status are sent as housekeeping information. Calibration is performed under ground command.

Figure 2.5 shows the appearance of the instrument prior to integration.

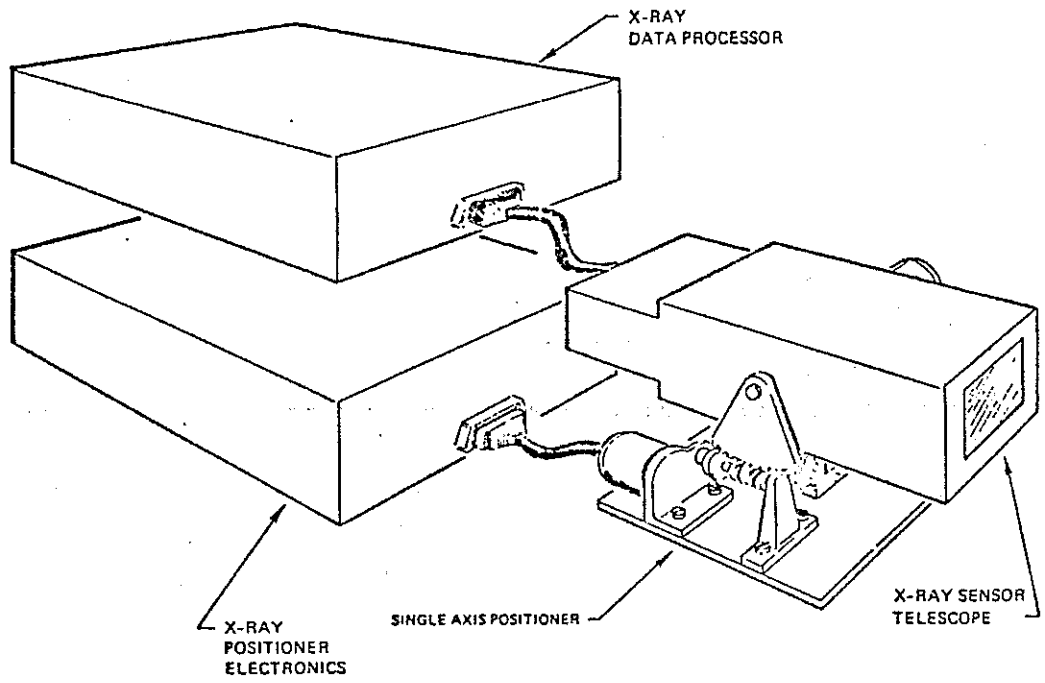

Figure 2.5 X-Ray Sensor System

Table 2.4 gives the telemetry output ranges, words, and rates.

Table 2.4 X-Ray Sensor Outputs

Measurement	Type	Measurand Range	Output Voltage Range	TM Word	Seconds/ Sample
X-Ray 0.5 to 3.0 Å Signal (X_2)	Analog	10^{-6} to 10^{-1} $\frac{erg}{cm^2 s}$	0.000–5.000	16	3.06
X-Ray 0.5 to 3.0 Å Bkgrd (X_4)		+2 to -8 x 10^{-12} amp		60 (7)	98.0
X-Ray 1.0 to 8.0 Å Signal (X_1)		10^{-5} to 1 $\frac{erg}{cm^2 s}$		18	3.06
X-Ray 1.0 to 8.0 Å Bkgrd (X_3)		+1 to -4 x 10^{-11} amp		60 (6)	98.0
Temp, X-Ray Sensor (X_{11})		-10 to 50°C		28 (7)	196.1
Cal Ref Voltage (X_{13})		3.85 V		60 (8)	98.0
Temp X-Ray Electronics (X_{12})		-10 to 50°C		28 (8)	196.1
X-Ray Elevation (X_{16})		-30 to +30°		60 (10)	98.0
Range, X-Ray 0.5 to 3.0 Å (X_7) (X_8)	Digital 2 bit each	Range 1 thru 4		15	3.06
Range, X-Ray 1.0 to 8.0 Å (X_5) (X_6)		Range 1 thru 4	"1": +2.4 to +5.5	15	3.06
			"0": -0.5 to +0.5	15	3.06
Cal/Data (X_9)	1 bit	Cal/Data		15	3.06
X Ray 0.5-3 Å Wide band Background (X_{14})	Analog	Preamplifier Outputs	0.000-5.000	52	3.06
X Ray 1-8 Å Wide band Background (X_{15})		*Normally observed in dwell mode only		64	3.06

3. THE SOLAR X-RAY INSTRUMENT

3.1 General

The function of the solar x-ray instrument is to provide broadband, whole sun measurements of the soft x-ray spectrum. Two bands ≃ 1-8 Å and 0.5-3 Å are employed to enable the hardness of the solar spectrum to be measured. Typical smoothed solar spectra are shown in figure 3.1.

The objectives of the sensor are to achieve a sensitivity to permit quiet sun background measurements at as low a level of solar activity as possible and permit the detection of events at the lowest practicable threshold for early event warning. It would also be desirable to be able to measure the spectrum of small events. However, as is shown in figure 3.1, the flux level in the 0.5-3 Å range may approach 2 orders of magnitude less than that in the 1-8 Å region, and its measurement may pose considerable instrumental difficulties. The requirements which were set for the sensor so as to meet these objectives are set forth in table 3.1. The flight instrument can theoretically meet all the design requirements and also the sensitivity goal (10^{-5} ergs cm^{-2} sec^{-1}) in the 1-8 Å band but not the goal in the 0.5-3 Å band.

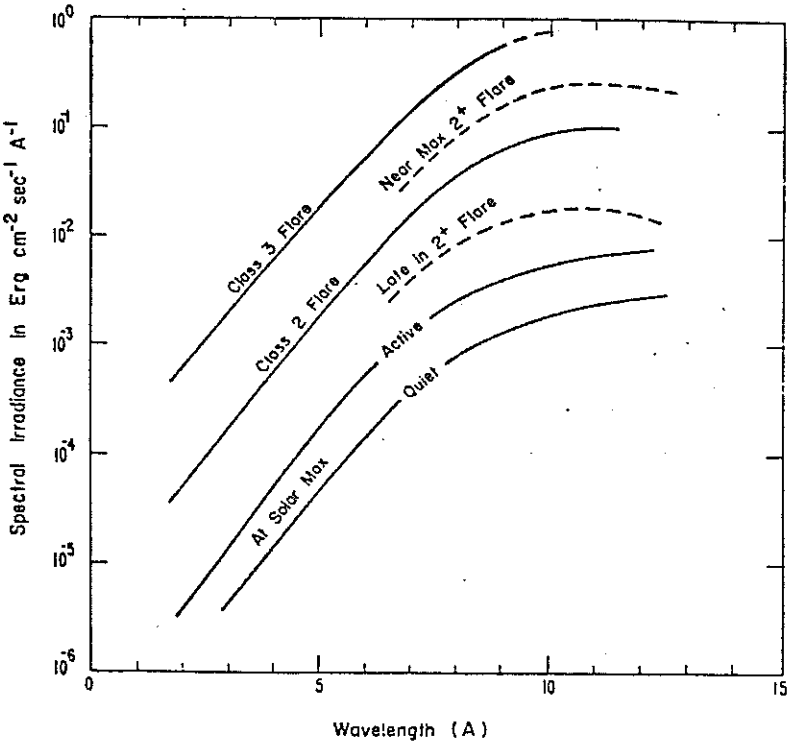

Figure 3.1 Representative X-Ray Spectra for Solar Flares. Lower Two Curves Indicate Solar Emission Under Nonflare Conditions. (With acknowledgment to H. Friedman, "Ultraviolet and X Rays from the Sun," Annual Rev. of Astron. and Astrophys., Vol. 1, 1963.)

Table 3.1 X-Ray Instrument Requirements

PRIMARY

- MONITOR SOLAR X RAY EMISSION IN 0.5-3 Å AND 1-8 Å BANDS
- DYNAMIC RANGE

	X-RAY FLUX (ERGS/CM² SEC)			
	DESIGN MINIMUM		DESIGN GOALS	
BAND	MIN	MAX	MIN	MAX
0.5-3 Å	10^{-6}	10^{-2}	10^{-7}	10^{-1}
1-8 Å	10^{-4}	10^{-1}	10^{-5}	10^{0}

- ACCOMMODATE ELECTRON ENVIRONMENT

E_e	>0.30	>0.45	>1.05	>1.90	MEV
$J(>E_e)$	2×10^7	7×10^6	7×10^5	1.5×10^5	e/CM² SEC

- RESPONSE TIME: < 30 SEC
- RESOLUTION: ≤ 10% OF FLUX BEING MEASURED
- HOUSEKEEPING SHALL BE PROVIDED TO VERIFY SENSOR STATUS AND RESPONSE TO BACKGROUND ELECTRONS
- SAMPLING RATE: ≥ 1 SAMPLE PER 10 SEC FOR EACH BAND

SECONDARY

- ACCOMMODATE TEMPERATURE RANGES OF EQUIPMENT PLATFORM

3.2 Choice of X-Ray Sensor

Three types of basic broadband x-ray sensor are available and were considered. All depend on the deposition of the x-ray photon energy in the form of ionization in a volume of gas. The photons enter through a thin metallic window whose transmissivity determines the long wavelength cutoff. The three types are differentiated by the way the initial ionization is collected and are:

1. The ion chamber
2. The proportional counter
3. The Geiger-Muller (GM) counter.

In the ion chamber, a pure fill gas is employed, and the ionization produced is collected without gas multiplication by a relatively low potential gradient, 10-50 V/cm, applied across the chamber. The output current is a measure of the rate at which energy is deposited in the gas.

In the proportional counter, controlled multiplication is used by applying sufficient potential gradient to create additional ionization by collisional processes. The amount of charge collected per photon is still proportional to the energy per photon, however, and individual photons can be counted and their energy determined. In the GM counter, the multiplication saturates so that all events produce the same quantity of charge at the output irrespective of the incident photon energy. In both the latter types, small amounts of organic gas are added to the basic gas filling to prevent continuous ionization and quench each event. The presence of these gases, particularly in the case of a proportional counter, leads to a limited lifetime. The ion chamber was, therefore, selected as the most likely to meet the 5 year lifetime goal for the satellite system, because it is a simpler materials system. The ion chamber does, however, have the disadvantage of requiring that the electronics system handle the small signal currents ($\simeq 10^{-13}$ A) produced at the required thresholds.

The basic ion chamber design follows broadly that used in the SOLRAD sensors. The efficiency of a chamber can be represented by

$$E(\lambda) = e^{-(n\rho x)}_{\text{window}} \left[1 - e^{-(n\rho x)}_{\text{gas}}\right]$$

where n is the appropriate mass absorption coefficient, ρ the density, and x the thickness. The mass absorption coefficients are not constants but known functions of wavelength. The parameters chosen for the chambers in the SMS instrument are:

0.5-3 Å	Window 20 mil beryllium Gas filling xenon at 180 mm Hg pressure.
1-8 Å	Window 2 mil beryllium Gas filling Argon at 800 mm Hg pressure.

The resulting efficiency versus wavelength for the two chambers is shown in figure 3.2. The wavelengths for 50% of peak efficiency are $\simeq$ 0.9-2.6 Å and 1.5-6 Å, respectively. However, there is no simple way of using these measurements to deduce the x-ray spectrum. The complete chamber response should be convolved with a spectral model whose parameters are then adjusted iteratively to provide a best fit to the data (Reference 3.1).

3.3 Instrument Concept

The geometry of the spin stabilized SMS with respect to the sun is shown in figure 3.3. For a nominal zero inclination geosynchronous orbit, a sensor viewing outwards from the satellite equatorial plane at the equinox will view the sun once per revolution for a period determined by its acceptance angle in that plane. Over the year, the angle between the sun satellite line and the equatorial plane will oscillate through the $\pm$ 23.5 corresponding to the earth's spin axis inclination to its orbital plane. The simplest possible arrangement for a solar x-ray sensor would be to use a fixed sensor with sufficient acceptance angle in the spin

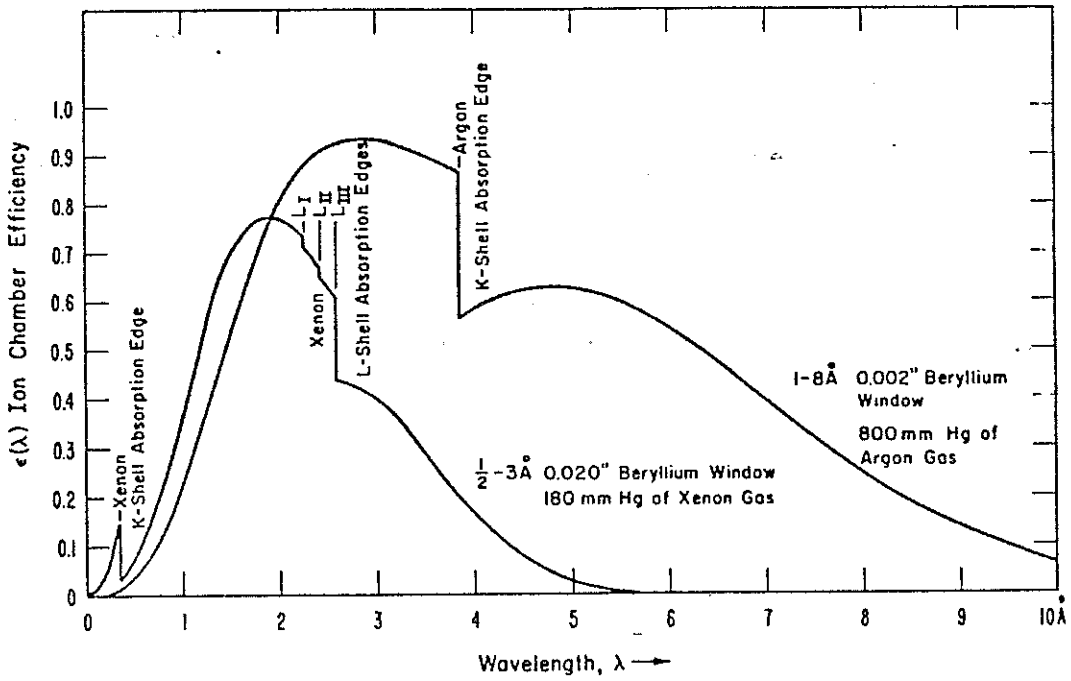

Figure 3.2 X-Ray Ion Chamber Wavelength Response

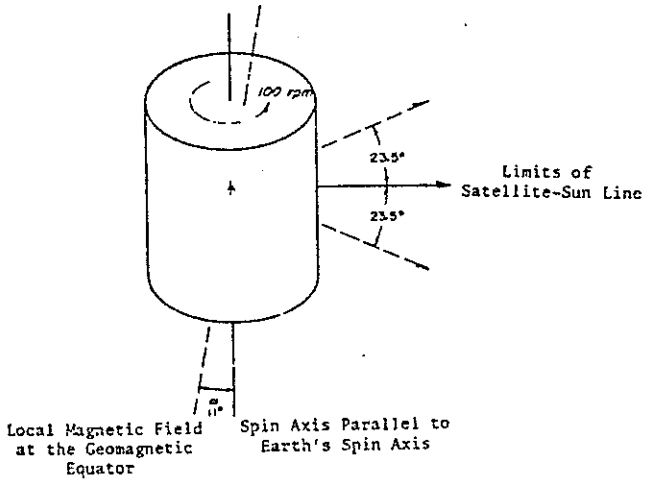

Figure 3.3 Basic SMS/GOES Satellite Geometry for Nominal 0° Inclination Orbit

axis plane to see the sun at all angles (Reference 3.2). The alternative, which proves to be desirable to limit the instruments sensitivity to the ambient electron environment, is to use a sensor with a smaller acceptance angle and provide a single axis pointer to enable the slow variation in sun angle to be tracked.

On the SOLRAD satellites, the current from the ion chamber is amplified and converted to a voltage by a suitable electrometer amplifier and telemetered to the ground by FM/FM telemetry with sufficient bandwidth to show each individual current pulse as the sensor views the sun. The electrometer zero and any additional ion chamber current due to energy deposited by electrons or other charged particles is immediately apparent as a baseline shift and can be subtracted from the data. The latter is an infrequent occurrence, however, since the SOLRAD orbit takes it below the earth's radiation belts for the majority of the time.

A different approach was necessary for SMS/GOES for two reasons:

1. The limited telemetry bandwidth ($\simeq 64$ bps) available to the total SEM from the geostationary orbit precludes transmission of the complete spin cycle with adequate sampling even if the whole bandwidth were allocated to one x-ray channel.

2. The large background currents which may be caused by the trapped electron environment would require an unnecessarily large dynamic range to accommodate the background and the signal simultaneously with sufficient resolution.

The decision was, therefore, made to design a signal processing system which would subtract the background and make a best estimate of the value of the solar flux using the information on the sun angle already available from the sun sensor and the Attitude Determination And Control (ADAC) subsystem.

3.4 The Electron Background Problem

The trapped electron background in geosynchronous orbit has been measured by a number of workers. The most convenient data for this problem is that accumulated by the Aerospace experiment on the ATS-1 satellite, since this has been reduced to a convenient statistical form (Reference 3.3).

A worst case electron environment for all local times and not exceeded for more than 5% of the time is described by the integral fluxes:

E_e	>300 keV	>450 keV	>1.05 MeV	>1.9 MeV
$J > (E_e)$	2×10^7	7×10^6	7×10^5	1.5×10^5

The electrons can interact with the x-ray sensor in two ways. Firstly, those electrons with energies sufficient to penetrate the window (≃1 keV for 2 mil and 3 keV for 20 mils) can deposit energy directly as ionization in the gas. Secondly, electrons absorbed or moderated in surrounding materials will give rise to bremsstrahlung photons which, if they reach the ion chamber, will give rise to signal current through the photoelectric capture and Compton scattering processes. For performance calculation purposes, two analytical spectrums were defined. For evaluating direct electron effects, one spectrum matched the ATS-1 data at high energies. For evaluating the bremsstrahlung effects, the second spectrum matched the ATS-1 data at low energies. For both spectra, the hardness matches that of the model environment given by Vette (Reference 3.4). These are, for direct electron effects:

$$N(>E) = 1.7 \times 10^{9}\ e^{-4.6E}\ cm^{-2}sec^{-1}$$

and for bremsstrahlung:

$$N(>E) = 2.8 \times 10^{7}\ e^{-4.6E} cm^{-2}sec^{-1},$$

where N is the isotropic flux for energies greater than E in MeV.

The direct electron influence on the ion chamber can be reduced by collimation so that only a small part of the isotropic flux can enter the collimator. It can then be further reduced by deflecting the electrons with either a magnetic or electric field so that those below some critical energy, dependent upon the field strength, are deflected so as not to reach the ion chambers. Use of collimation in the equatorial plane of a spinning satellite with a fixed detector must be considered in a trade off with the desired signal, which is also reduced by the collimation.

The bremsstrahlung effects can be reduced by using a combination of low Z shielding materials which minimize the production of x-ray photons together with inner shielding of the system with high Z material to absorb those x-ray photons which are produced.

A steady background current in the ion chamber due to electrons increases the noise background against which the solar x-ray signal must be distinguished. The effect is similar to the shot noise in a thermionic diode operated under temperature limited conditions such that each electron emitted constitutes an independent event. In this case, for an integration time T, the rms uncertainty is given by

$$I_n = \sqrt{N}.QT^{-1}$$

where N is the number of independent events and Q is the charge resulting from each event.

Two other properties of the electron environment are important. These are the degree of anisotropy and the time variability of the flux. Practical measured data on either of these properties is insufficient for design purposes. The degree of anisotropy is important because it introduces spin modulation into the background electron current which will, in general, introduce an error into the estimate of the solar x-ray flux. The assumption that has been made is that the pitch angle distribution with respect to the magnetic field direction is sinusoidal. For the nominal inclination of a dipole field with respect to the satellite spin axis (11°), there would be a peak-to-peak modulation of approximately 2% repeating once or twice per satellite revolution. Time variability of the electron flux becomes significant if there are significant changes within a spin period, or if it is longer, the period within which the background subtraction process is implemented.

3.5 Basic Sensor Design

The basic design of the sensor is illustrated in figure 3.4. The concept is that of a single rectangular collimator serving ion chambers for both energy ranges. At the mid point of the collimator are the pole pieces of a magnet which produces a field in the satellite equatorial plane to deflect electrons away from the ion chamber. The angular acceptance angle in the spin axis plane is designed to be just sufficient to provide full illumination of the ion chambers by the solar disc (0.6° full angle) for displacements of the disc center of ± ½° from the nominal axis which allows for reasonable misalignment and step quantization in the pointer. The loss in sensitivity due to misalignment is shown in figure 3.5. The remaining parameters were determined in a study directed at optimizing the instrument signal to noise ratio with respect to both the direct electron and bremsstrahlung background intensities versus the variable parameters in the instrument design such as the collimator dimensions, magnet weight, etc., within the overall constraint of the weight and volume limit for the instrument (Reference 3.5).

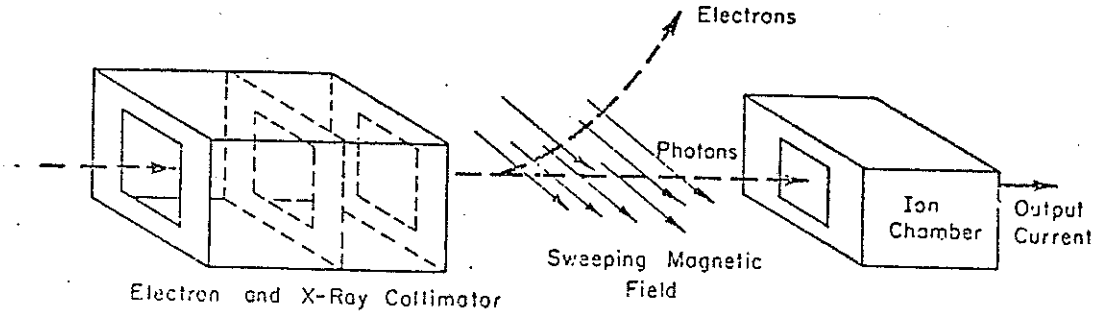

Figure 3.4 X-Ray Telescope, Conceptual Design

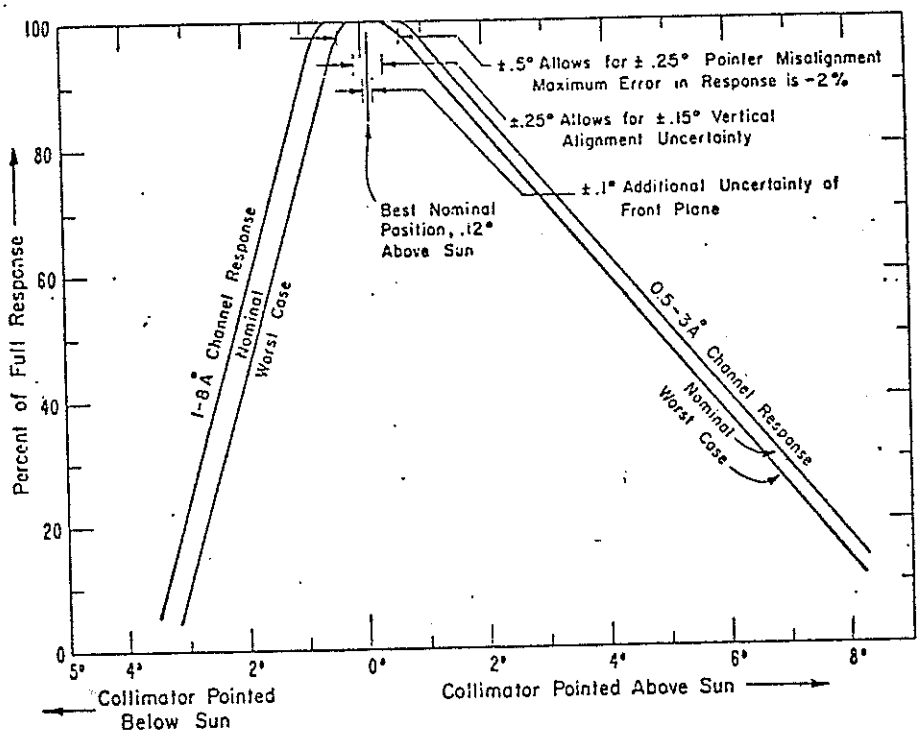

Figure 3.5 Angular Response of the X-Ray Telescope in the Spin Axis Plane (the effect of the baffles is not included)

A photograph of the actual flight instrument is shown in figure 3.6. The telescope assembly is mounted on a single axis pointer and consists of the collimator, which limits the field of view of the instrument, the dual ion chamber assembly, and the electrometer preamplifiers mounted on the rear of the ion chambers. The magnetic field for deflecting incoming electrons is provided along the telescope rotation axis by a fixed magnet and pole piece assembly. This arrangement minimizes the inertia of the moving system and also prevents changes in telescope angle from affecting the magnetometer measurements. The main signal processing electronics are contained in a separate box. The single axis positioner is driven by a bidirectional stepping motor providing a range of >±25° in 0.25° steps. The cycle memory for the motor drive is held by latching relays so that the correct command response can be made even after interruptions to the power to the system. Telescope position readout is provided by a linear transformer shaft angle sensor which provides a 0-5 V output to telemetry.

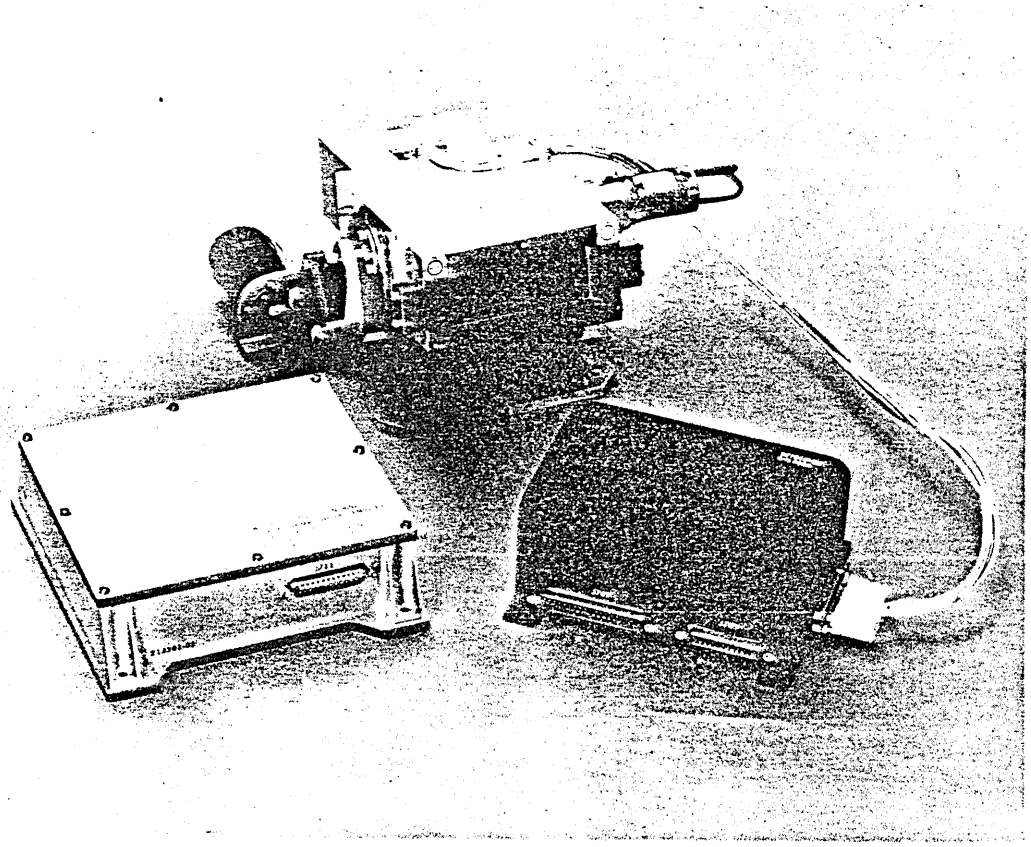

Figure 3.6 X-Ray Instrument

3.6 Collimator Design

A detailed cross section of the collimator and ion chamber assembly is shown in figure 3.7. The ion chambers, which extend the full width of the collimator in the spin plane, are stacked one above the other with the short wavelength chamber occupying the lower position and having the larger entrance aperture. The entrance baffles are intended to collimate the incoming electrons and provide the maximum protection to the short wavelength chamber which has the lower design threshold. Electrons deflected upwards by the magnet are absorbed by the ridge structure. This together with other surfaces which define the collimation are of combination low and high Z material to minimize bremsstrahlung production in the first instance and then to absorb photons exiting in the direction of the ion chambers.

Computer calculations of the threshold for energetic electrons were performed by individual electron tracing using a predetermined set of incident electrons and exploiting symmetry to the maximum extent. The threshold,

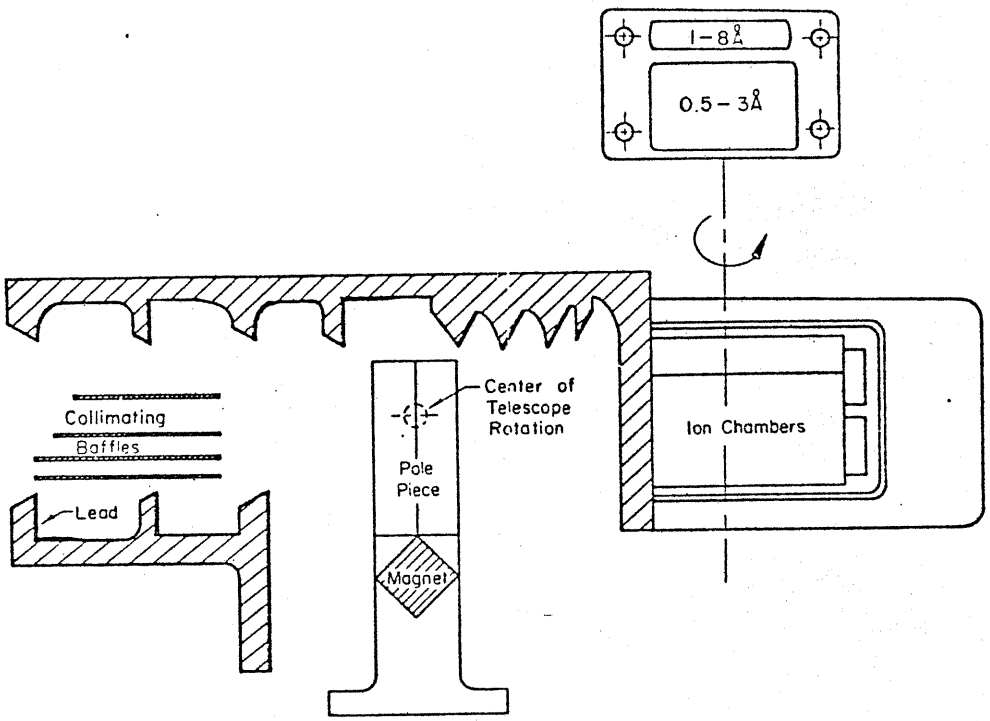

Figure 3.7 Collimator and Ion Chamber Design

defined as the energy at which 50% of the set reached the chamber window, was found to be ≃ 2 MeV for the short wavelength chamber and ≃ 1.5 MeV for the long. The threshold for the single electron channel in the EPS was selected to be 2 MeV to provide an approximate independent monitor of the incident flux of the electrons which could reach the ion chamber interior An attempt was also made to directly measure the electron rejection efficiency using an electron accelerator source. Considerable practical difficulties existed, but the results are reasonably consistent with the calculations (Reference 3.6).

3.7 Electronics Design

3.7.1 Signal Processing Design

Each time the sun sweeps through the angle of view of the collimator, the total illumination of the ion chambers is a symmetrical trapezoidal function of time with a full width of ≃80 ms and a width at full amplitude of 37 ms at the nominal 100 rpm spin rate and at a 0° look angle. On this time scale, the ion chamber response at the bias used is essentially instantaneous. The pulse of current due to the sun will be superimposed on a background current due to electrons which reach the ion chamber interior.

In an isotropic electron environment, this current would not be a function of spin angle but only of the changing environment and would be relatively straightforward to remove in the signal processing electronics. However, due to the local magnetic field, the electron environment will be anisotropic exhibiting some form of minimum in a loss cone parallel to the field with a maximum in directions perpendicular to the field. Due to the inclination of the satellite spin axis to the field direction ($\leq 11°$ for a dipole field), and the inclination of the sensor to the spin plane, the sensor will scan out some portion of this anisotropic distribution in each spin cycle giving rise to a current modulated at one or two times the spin rate. The degree of anisotropy is likely to vary considerably from time to time as geomagnetic conditions vary and as the satellite moves in local time into different regions of the magnetosphere. Thus the total current due to all these effects is expected to be of the form shown in figure 3.8. The signal processing scheme used to obtain an estimate of the solar component embodies the following philosophies:

1. On board extraction of the solar induced signal from the background at as early a point in the chain as practical to minimize the dynamic range requirements.

2. Extraction from background on a pulse by pulse basis before signal integration to minimize the effects of temporal fluctuations in the background.

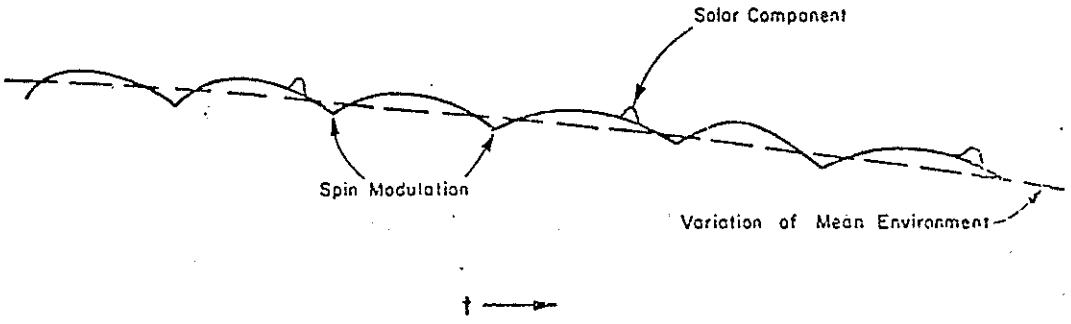

Figure 3.8 General Expected Form of the Ion Chamber Current

The basic scheme used is shown in figure 3.9. The signal from the ion chamber is amplified and shaped by an electrometer preamplifier which combines a single pole low pass and high pass response. The high pass response is obtained by overall feedback via a high gain integrator stage to a summing resistor which is designed to directly cancel the mean value of the chamber current with enough current capability to deal with the maximum electron induced current theoretically predicted for the sensor in the specified natural background. The low pass response is obtained by the RC combination in the main gain determining feedback path to the summing point. Background subtraction is mechanized by the FET switches S_1 and S_2. Normally S_1 is closed and S_2 is open. The capacitor C_1 is

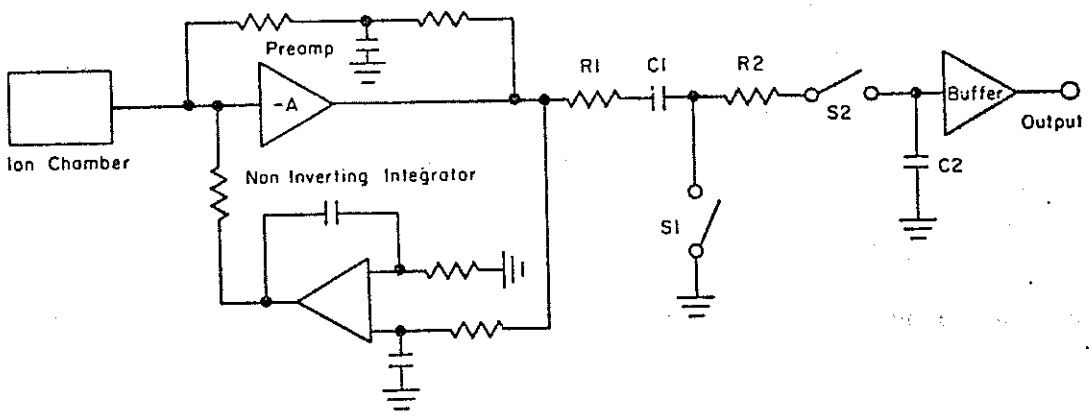

Figure 3.9 Basic Background Subtraction Signal Processing Scheme

maintained charged to the output voltage of the input preamplifier with only a small lag due to the series resistor R_1. When the sun pulse arrives at the gates, the switch positions are reversed and the signal, now starting from zero due to the bias remembered by C_1, is coupled into the signal integration R_2C_2 which functions with a 3 second effective time constant. Thus the signal is extracted from the background existing just before the start of the sun pulse. The values of the filter time constants used were determined in a computer model study which compared the noise performance of this signal processing scheme with an ideal gated integrator scheme using very long term background averaging before subtraction. A broad optimum was found using the simple single pole filters with a -3 dB pass band of 1.6-9.6 Hz. With the optimum filter, the noise performance was found to be only degraded by a factor of 0.6 compared to the ideal gated integrator which would, of course, have had an unacceptable response to spin modulation and electron background changes. More complex filtering schemes could have been devised to reduce the response to spin modulation and temporal changes, but the gain was small and the practical complication outweighed the advantages (Reference 3.7).

3.7.2 Signal Electronics

A block diagram of the complete instrument is shown in figure 3.10. To cover the required dynamic range, the input preamplifier is switched, in gain by a factor of 100, and the post demodulator attenuator is switched by a factor of 10. The range switching logic (not shown) operates by comparing the post amplifier output against a high and low reference limits and commanding appropriate range changes when required. Hysteresis is incorporated to prevent frequent changes of range when operating close to the limit of one range. The two scale bits generated by the range switching are telemetered in word 15, bits 6 and 7 for the short wavelength

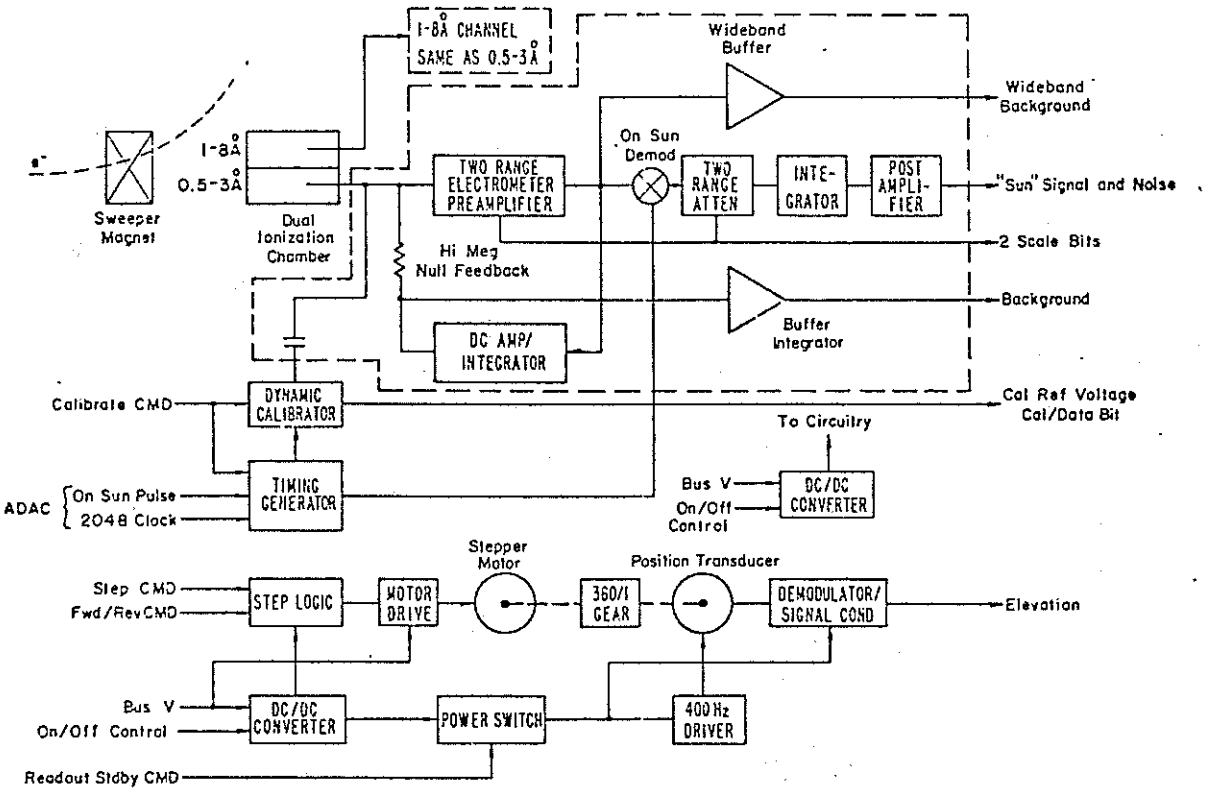

Figure 3.10 SMS X-Ray Instrument Block Diagram

channel and bits 8 and 9 for the long wavelength channel, the MSB being first in each case. The demodulator and integrator have been described in more detail in the previous section.

Two "background" outputs are telemetered as an aid to evaluating the effects of electron induced ion chamber currents. The normal background channel is carried in the 32 channel submultiplexer in words 6 and 7 for the short and long wavelength channels, respectively. This represents the mean value of the ion chamber current (including the solar contribution) obtained from the voltage across the background null feedback resistor. The calibration of this output is not affected by the instrument range switching. Since the pass band of the nulling feedback is such as to include significant components at the satellite spin frequency, the telemetry output is buffered through an RC filter having an effective low pass time constant of 2.5 sec to attenuate the spin frequency components and be more consistent with the sampling period of 1.64 minutes.

To evaluate the spin modulation of the background a second "wide band background" output is provided which appears in the telemetry main frame on words 52 and 64 for the short and long wavelength channels, respectively. The signal is obtained directly from the output of the electrometer preamplifier and is changed in sensitivity by that amplifier's range switching.

These words are primarily intended to be utilized in the telemetry dwell mode which provides a sampling rate of ≈ 20 per second, adequate to resolve spin related effects. In the nondwell mode, the amplitude distribution statistics (e.g., mean and standard deviation) may be obtained by averaging over a period providing that the signal is stationary and that the spin rate is not such as to be synchronous with the telemetry rate. In principle, again with the same conditions, the time history can be reconstructed if a spin reference is available or can be constructed on the ground.

To relate the wide band background output V_o to the actual ion chamber current I requires that the observed signal be unfolded back through the preamplifier response function.

Timing for the demodulator switching and also for the onboard electrical calibration system comes from the Timing Generator which is provided with the 2048 pulse spin clock signal and an "on sun" pulse from the ADAC subsystem.

The onboard electrical calibrator enables the performance of the whole amplifier and demodulator system to be checked and also an "off sun" zero reference established. On receipt of a calibrate command, the timing generator changes the demodulator timing by 180° so that the instrument looks away from the sun. Since the electron contamination effects are expected to be approximately symmetrical about 180°, this enables a true off sun reference to be established which includes any particle effects present. Simultaneously a sequence of simulated sun signals is injected into the signal chain in parallel with the ion chamber output. This signal is produced by applying a symmetrical ramp voltage through a small capacitor connected to the preamplifier input. The timing, voltage slope and duration, and capacitor value are chosen so that a rectangular current pulse of appropriate value and timing to simulate the ion chamber solar output is applied to the system during the first half of the ramp signal. During the second half of the ramp signal, an equal current pulse but of opposite polarity is produced. Since at this time the demodulator has completed its cycle, this has no effect on the instrument output. A correction is made in referencing the calibration current to the ion chamber current, however, for the use of a rectangular rather than the actual trapezoidal current pulse produced by the sun. The sequence of calibration levels produced simultaneously in both channels is as follows. Note that the instrument range setting is forced during the sequence so that zero readings can be obtained on all ranges. The 8 step cycle takes approximately 40 seconds per step and is terminated only when a calibrator off command is received. The first step in the sequence after the calibrate command will be truncated.

1. Scale 4 upscale
2. Scale 4 no signal
3. Scale 3 upscale
4. Scale 3 no signal

5. Scale 1 upscale

6. Scale 2 upscale

7. Scale 2 no signal

8. Scale 1 no signal

The calibration values for a particular instrument must be referenced to baseline values obtained during bench calibrations and subsequent pre-launch operation. Since the calibration ramp is obtained from relatively simple and stable circuits compared with the rest of the instrument, it can normally be regarded as calibrating the electrical gain of the instrument. The electrical reference voltage which determines the ramp slope and voltage limits is telemetered in word 8 of the 32 channel submultiplexer to confirm the stability of the calibrator. The reference voltage is therefore only present during calibration.

3.7.3 Positioner Drive and Power Control

The block diagram in figure 3.10 also shows the positioner drive electronics. The system is a conventional stepping motor driver which is controlled by ground command to index one step either forward (towards the +Z axis) or reverse. The 90° stepping motor is geared by 360:1 to the telescope to provide 0.25° steps. The position of telescope is sensed by a linear transformer shaft angle sensor. The associated electronics provide a nominal 0-5 V readout of elevation angle over the ±25° range. To conserve power on the satellite the readout section of the electronics may be commanded off independently of the step control logic. This latter logic contains latching relay memories of the step sequence so that the power to the whole telescope positioner electronics may be interrupted without resulting in initial anomalous responses due to the step memory being misaligned with the motor position. Both the x-ray electronics and the positioner electronics power is removed in the satellite eclipse mode of operation. In the off mode, all bilevel outputs from the instrument read high. An unambiguous "on" indication can be obtained from the wide band background channels which reside at zero for power off and at ≃±2.5 V for power on.

3.8 Overall Instrument Calibration

The overall instrument calibration is obtained from the sum of independent calibrations of the ion chamber x-ray flux to current efficiency and direct electrical calibration of the signal electronics. Overall x-ray flux to telemetry output calibrations have been provided for each flight instrument by the contractor (Reference 3.8). These are based on a calculated ion chamber efficiency. Separate calibrations of the flight ion chambers efficiency and wavelength response have been made by SEL in collaboration with the Naval Research Laboratories (Reference 3.9). The contractor calibrations should be corrected to allow for the difference between these two values if necessary. Calibration of the elevation angle readout is provided for each instrument by the contractor (Reference 3.8).

4. ENERGETIC PARTICLE SENSOR (EPS)

4.1 Requirements

The original requirements for the Energetic Particle Sensor arose primarily from the need to monitor the radiation hazard to manned and unmanned operations in space, and the ionospheric effects at high latitudes, from solar protons and alpha particles produced during large flares. At the time the specifications for the SMS were defined, the performance requirements were expanded to reduce the lower limit of coverage for protons from 4 MeV to 1 MeV for protons and from 20 MeV to 4 MeV for alphas. This was done because of the increasing understanding of the role of trapped particles in this and lower energy ranges in the magnetic substorm process.

The performance requirements are summarized in table 4.1. In line with the radiation hazard mission, the sensors were required to measure the omnidirectional flux. However later some compromises with this objective was allowed to permit better resolution at the lower energies. The single electron channel was intended primarily to provide an independent monitor of the electron environment critical to the x-ray sensor performance, and the threshold of this channel was adjusted to match the expected sensitivity of the x-ray instrument.

Table 4.1 EPS Performance Requirements

- OMNIDIRECTIONAL SENSITIVITY
- PROTON FLUX 1-500 MeV; 7 INTERVALS LOGARITHMICALLY DIVIDED
- ALPHA FLUX 4-400 MeV; 6 INTERVALS LOGARITHMICALLY DIVIDED
- ELECTRON FLUX ≥ 0.5 MeV (ENERGY THRESHOLD ADJUSTABLE)
- DETECTOR GEOMETRIES, ELECTRONICS, AND TELEMETRY ACCOMMODATE RANGE BETWEEN COSMIC RAY BACKGROUND AND SOLAR EVENTS; AMBIGUITIES BECAUSE OF COUNTER OVERFLOWS AVOIDED
- EACH PARTICLE TYPE/ENERGY CHANNEL SAMPLED AT LEAST ONCE EVERY 24 SECONDS

In order that the instrument response should be unambiguous in large solar events, a somewhat arbitrary "largest solar event" was defined. Figure 4.1 shows this spectrum compared with estimates which have been made by various workers (Reference 4.1) of the giant solar events which took place in February 1956 and November 1960 and also an alternative spectrum which matches the envelope of these two events.

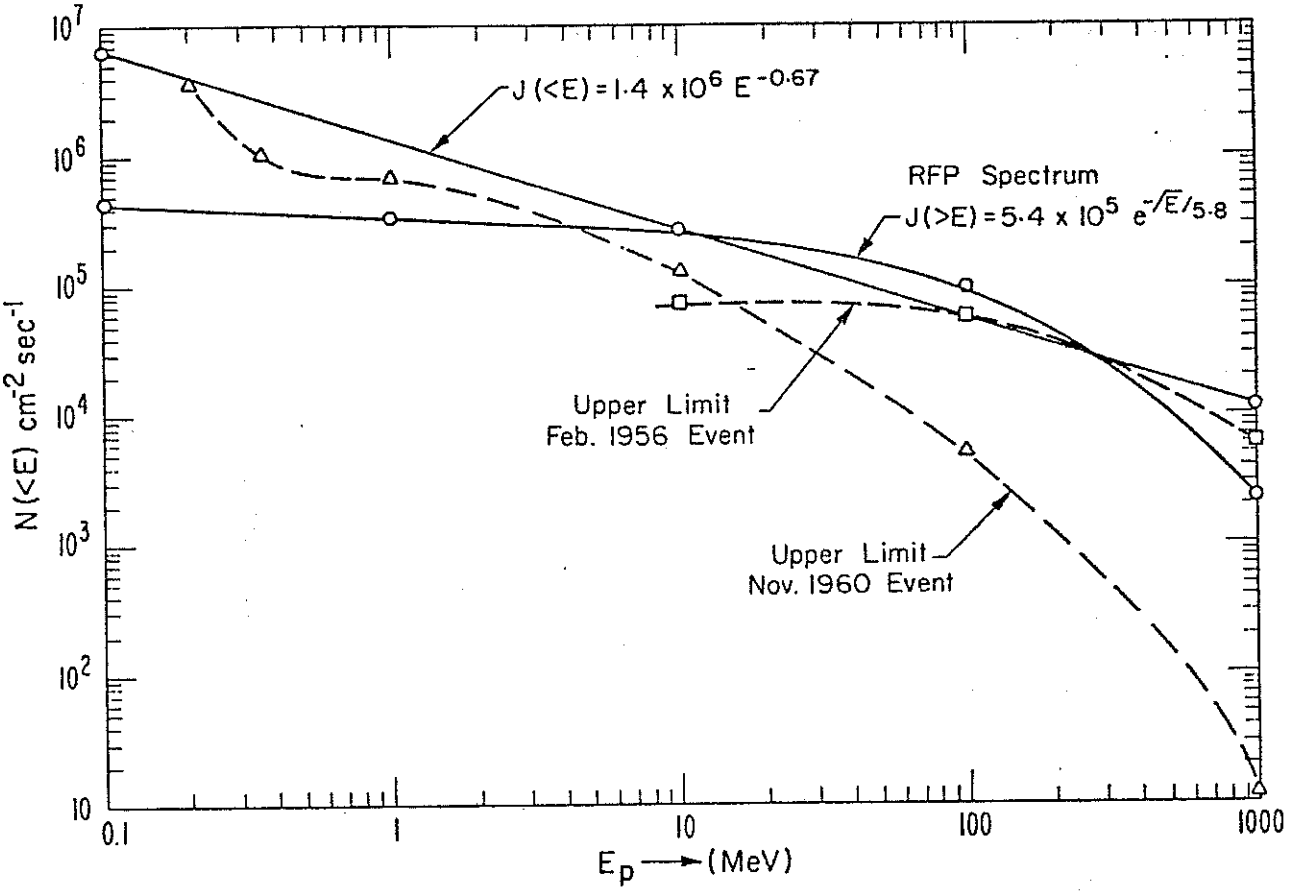

Figure 4.1 "Largest Solar Event" Spectrum

A further constraint which was placed on the design was that a system utilizing multiple separate detectors and parallel electronic channels was to be preferred over one depending on complex multidetector arrangements and electronic coincidence detection because of the greater protection against complete failure.

4.2 Description of the Instrument

The instrument can, for convenience of description, be split into two sections depending on the detector configuration employed. The high

energy channels (15 to 500 MeV for protons and 60 to 390 MeV for alphas) are derived from nominally omnidirectional cubical silicon detectors contained within a moderator dome assembly. The lower energy channels are derived from a telescope arrangement of 2 planar silicon surface barrier detectors which measures the flux in an approximately ± 25° angle about the satellite equatorial plane. A summary of the instruments channels and geometric factors has been given in table 2.2.

The two detector assemblies, each with a preamplifier included for each detector, are mounted on the satellite equipment platform looking out through cutouts in the solar panel array. The signal processing electronics are broken into two parts for convenience in packaging and also for isolation. All the pulse analog electronics up to and including the level sensors are contained in the Signal Analyzer Unit. The particle categorization logic, multiplexer, compression accumulators, and the calibrator are contained in the Data Processor Unit. Figure 4.2 shows a photograph of the complete EPS subsystem. An overall block diagram of the subsystem is shown in figure 4.3.

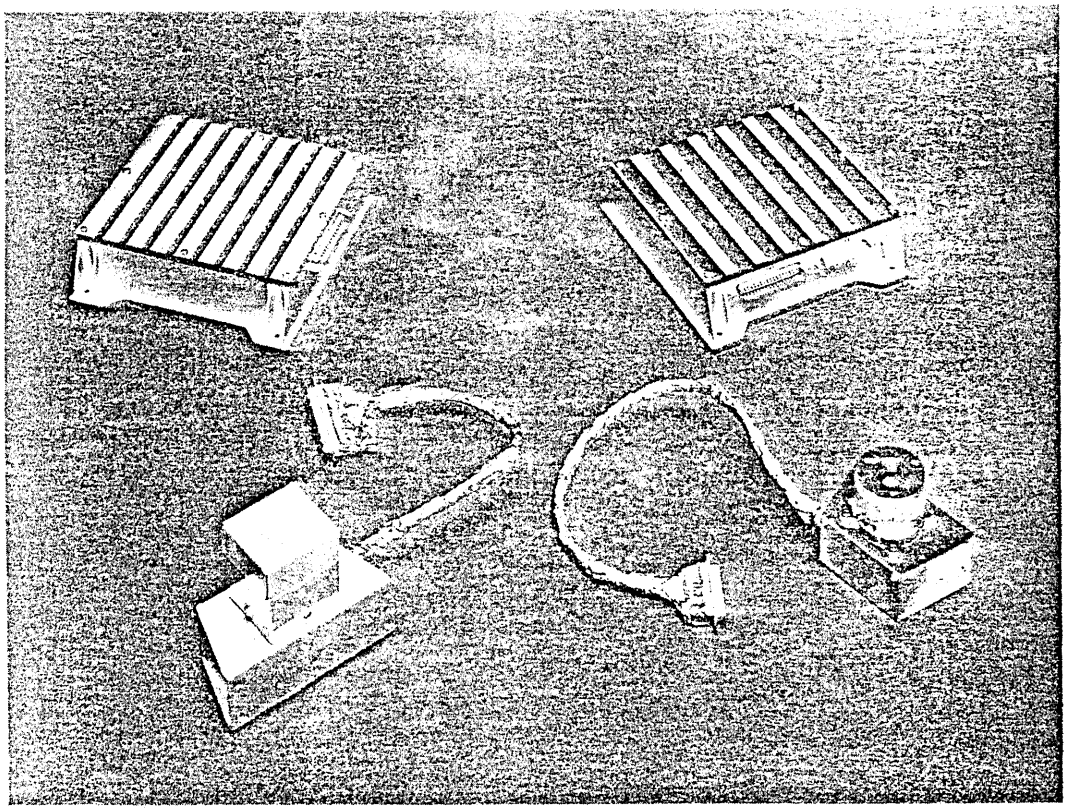

Figure 4.2 EPS Subsystem

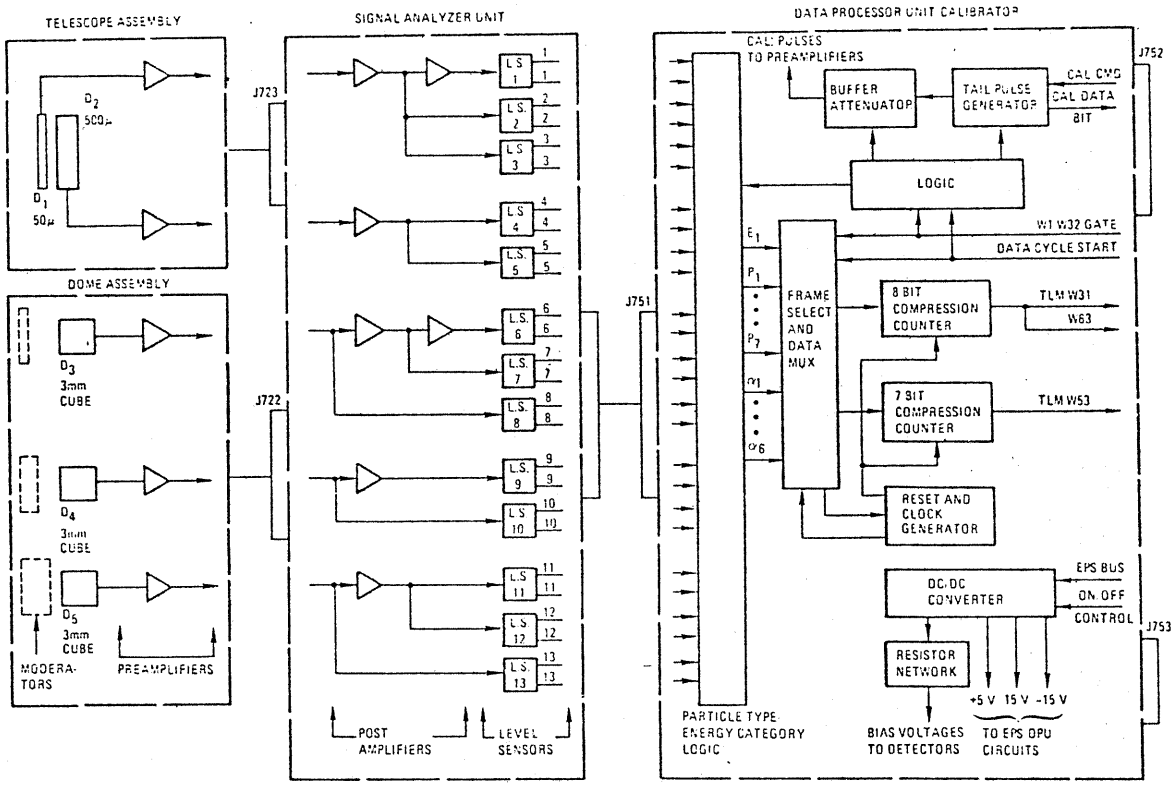

Figure 4.3 SMS-SEM EPS Block Diagram

4.2.1 The Telescope Detector

The low energy channels P_{1-3} and α_{1-3} are derived from a two detector telescope. The arrangement of the detectors is shown in figure 4.4. The front aperture is shielded by a nominal 2 μ thickness nickel foil which introduces an energy loss of ≃ 400 keV for protons. The foil stops electrons below ≃ 26 keV, thus reducing the possibility of random pileup events producing incorrect proton responses and also serves to shield the D1 detector from sunlight. The D1 detector is a nominal 50 μ thickness, and D2 is a nominal 500 μ thickness surface barrier silicon detector. Both detectors are nominally 100 mm^2 in area. The acceptance angle for channels derived only from the front detector (P1 and α1) is ≃88° and for all other telescope channels, P_{2-3} and α_{2-3}, is ≃ 56°.

Figure 4.5 shows the coincident pulse height response for the two detectors and the level sensor settings. This is a plot of energy deposited in D1 versus deposited in D2 with the independent variable of incident particle energy which is indicated along each plot. Characteristics are shown for both protons and alpha particles. The level sensor settings for D1 are shown by the horizontal lines and for D2 by the vertical lines. Logical combinations of these level discriminators represent particular areas on the plot and accept particles corresponding to those parts of the response passing through that area.

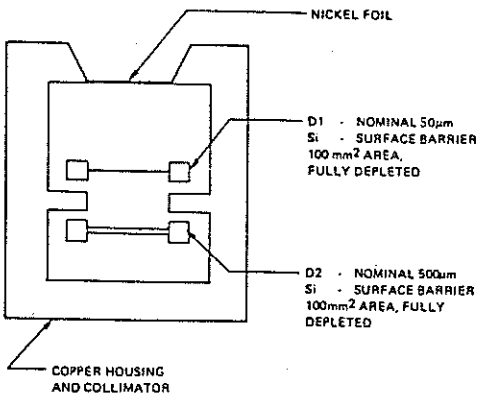

Figure 4.4 Schematic Representation of Telescope Assembly

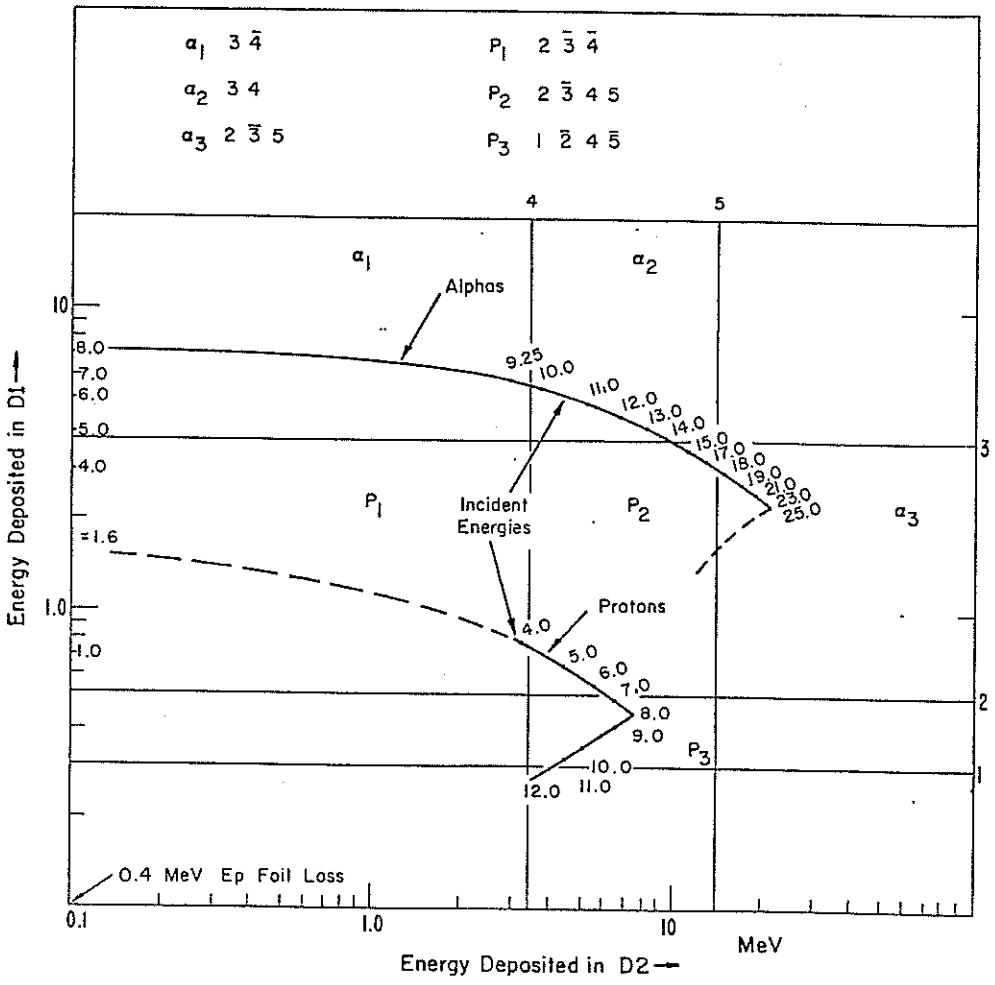

Figure 4.5 Pulse Height Response

The proton characteristic commences for particles not penetrating D1, and therefore not depositing energy in D2, along the vertical axis. The deposited energy is the incident energy less the ≃ 0.4 MeV lost in the foil. At ≃ 1.6 MeV incident energy the characteristic departs from the ordinate as the protons penetrate D1 and commence to deposit energy in D2. Channel P1 is formed by the logic 2 $\overline{3}$ $\overline{4}$ with level sensor 2 at ≃ 0.5 MeV and has a nominal response from 0.8 MeV to 4 MeV. Channel P2 with logic 2 $\overline{3}$ 4 $\overline{5}$ has a nominal response from 4 to 7 MeV with level sensor 4 set at ≃3.3 MeV. Channel P3 is defined by the logic 1 $\overline{2}$ 4 $\overline{5}$ and nominally responds to protons between 7 and 12 MeV. The break and reversal of the characteristic at 8 MeV are due to the penetration of protons through detector D2. Secondary responses to α particles exist in channels P1 due to low energy alphas in the range of ≃ 1-4 MeV and in P2 for alphas in the 15-17 MeV range due to alpha characteristic slightly intersecting the P2 area. These effects can be corrected for in analysis if necessary.

Channels α_1, α_2, and α_3 are formed in a similar way to that described for protons using in addition level sensors 3 and 5 at ≃ 3.5 MeV and 15 MeV, respectively. It was originally planned to set level sensor 3 at a slightly lower energy to just eliminate the α contamination of channel P2. However a small cross talk effect in the flight electronics caused level sensor 3 to become more sensitive when level sensor 5 was active and transferred events properly in α_3 to be counted in α_2. Level sensor 3 was readjusted to remove this effect.

The performance of the telescope sensor is in general fairly close to that predicted by simple theory. Some anomalies do exist in the calibration data which are due to a small percentage of sneak paths which exist for particles to enter D1 outside the normal active region and give rise to anomalously low charge collection. Also the spread of path lengths allowed in D1 are somewhat greater than are usually the case in telescope design. However these disadvantages are the result primarily of the attempt to provide as wide an acceptance angle as possible to be consistent with the original objective of isotropic instrument response.

4.2.2 The Dome Detectors

The arrangement of the detectors and moderator are shown in figure 4.6. The design is an extension of that used in the ATS-1 Omnidirectional Proton Spectrometer (Reference 4.2). The silicon detectors are cubical in form with a nominal active region 3 mm on a side. The detectors view a sector of a sphere (D5) or a sector of a hemisphere constructed on the satellite equatorial plane (D3 and D4). The satellite spin about the axis of the sectors completes an integration over 4 π or 2 π steradians, respectively. In the latter case, symmetry about the satellite equatorial plane, which is nearly perpendicular to the local magnetic field, is invoked to obtain an omnidirectional flux measurement. Each of the three detectors is shielded by a different nuclear thickness of moderator to provide the basic lower thresholds for protons of 16, 36, and 80 MeV for D3, D4, and D5, respectively.

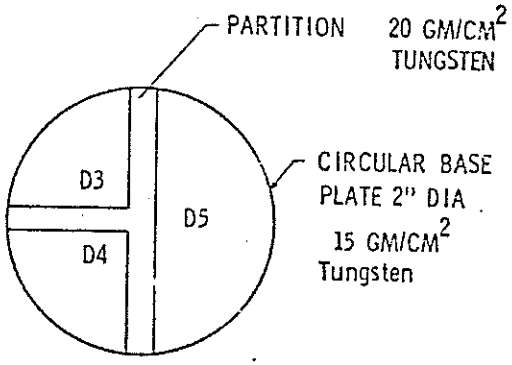

APPROPRIATE MODERATOR MATERIAL TO COVER EACH SECTOR

D3-D5: 3mm CUBICAL Si (Li) DETECTORS

Figure 4.6 Dome--Top View, Schematic Representation

Figures 4.7, 4.8, and 4.9 show the nominal incident energy versus deposited energy characteristics for each of the three detectors and the associated level sensor settings. The characteristics are plotted for a nominal 3 mm thickness in each detector. In each case, the initial rapid rise in deposited energy corresponds to the particles just able to penetrate the moderator. Only a very small increase in incident energy is then required for the remaining energy to be sufficient for the moderated particle to fully penetrate the 3 mm silicon path. For further increase in incident energy, the deposited energy falls and permits energy discrimination based on the rate of energy loss (dE/dx).

From D3, three level sensors, 6, 7, and 8, are employed. LS7 set at approximately 10 MeV defines the channel P4 proton response 16 to 36 MeV nominal using the logic 7 $\overline{8}$. Level sensor 8, set at ≃ 40 MeV defines the alpha channel response α_4 from 60 to 148 MeV nominal level. Level sensor 6 set at ≃1.6 MeV defines the electron channel response E1 of ≥2 MeV. This channel has a secondary response to protons ≥10 MeV.

From D4, two level sensors, 9 and 10, are used. LS9, set at ≃ 1.5 MeV, defines the proton response P5, 36 to 500 MeV nominal using the logic 9 $\overline{10}$. LS10, set at ≃ 30 MeV, defines the alpha response α_5 from 148 to 244 MeV nominal.

From D5, three level sensors 11, 12, and 13, are used. LS11 set at ≃ 2.7 MeV, and LS12, set at ≃ 2.7 MeV, define two proton channels, P6 and P7, with ranges 80 to 200 MeV and 200 to 500 MeV nominal using the logic 12 $\overline{13}$ and 11 $\overline{12}$, respectively. LS13, set at ≃ 33 MeV, defines the alpha channel α_6 with a response from 325 to 390 MeV nominal.

The actual responses of the channels from this detector system in practice are far from ideal rectangular pass bands, and the data from

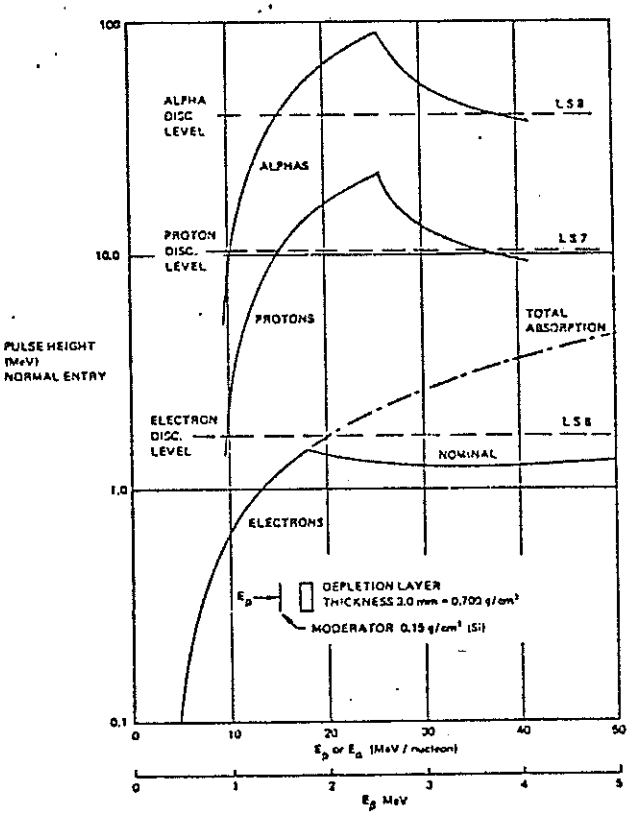

Figure 4.7 D3 Response

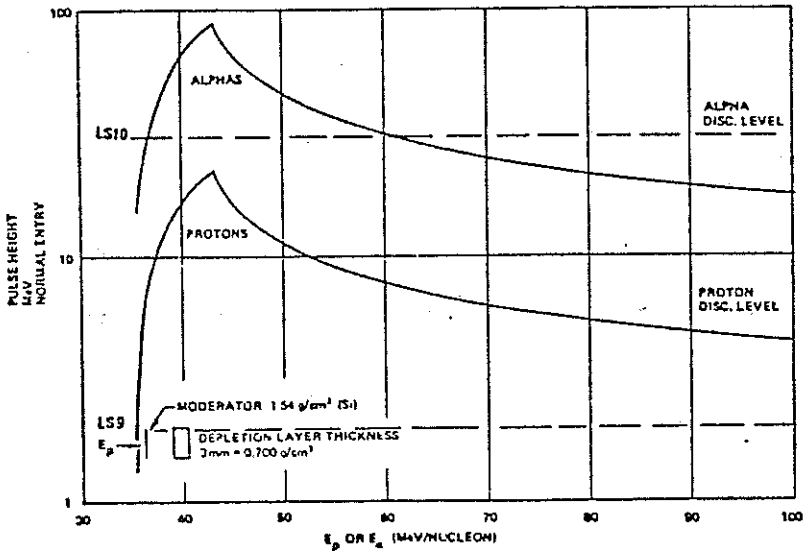

Figure 4.8 D4 Response

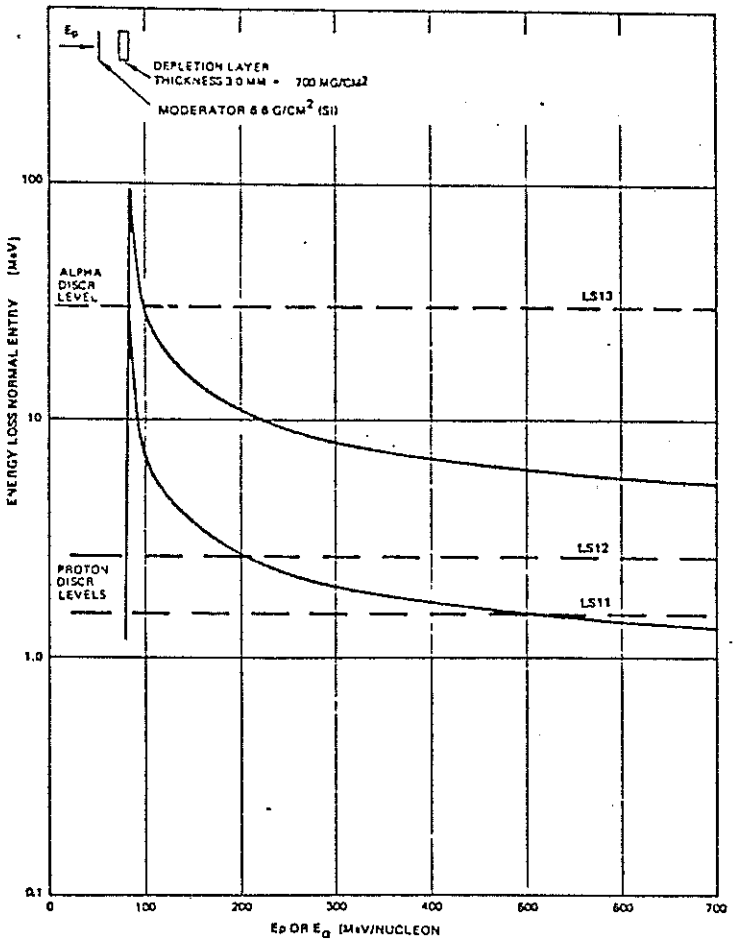

Figure 4.9 D5 Response

them must be used with some understanding and caution. There are two reasons for this, one expected and the other unexpected. Firstly, the second part of the deposited versus incident energy characteristic following the maximum deposited energy depends on the path length in silicon available to the particle. For an ideal cubical detector, the probability distribution of path lengths for random incidence is approximately rectangular, extending from zero to the maximum possible diagonal distance. Thus discrimination by level sensors in the dE/dx portion of the characteristic results in efficiency versus energy responses which will cut off slowly and approach zero response on the high energy side only for particles of the minimum ionizing energy. Thus the theoretical response for channel P7 which depends on two discriminators operating in the dE/dx region has the theoretical form shown in figure 4.10. Responses of this form can, of course, still be used to estimate the incident particle spectrum, but more analysis is required and care must be exercised in intuitive interpretation.

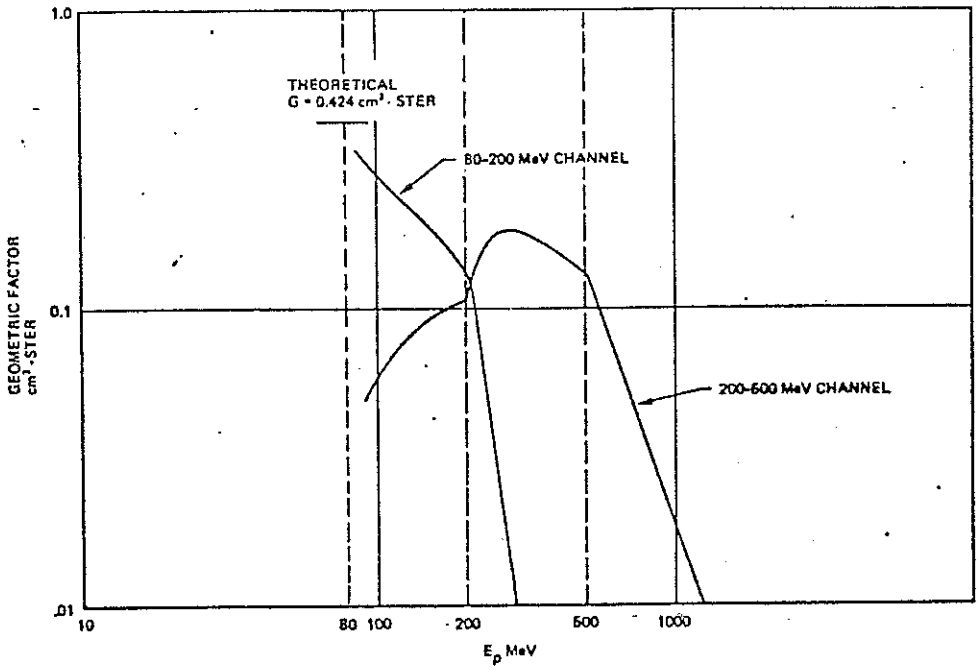

Figure 4.10 Efficiency vs. E_p for 80-200 and 200-500 MeV Channels

The second reason for caution in interpretation only became apparent during accelerator calibrations of the system. It was found that many of the cubical detectors exhibited an anomalous "secondary peaking" effect in which the distribution of pulse heights from the detector when exposed to a collimated beam of protons at a much higher energy than required to penetrate the 3 mm thickness showed many events in which much less than the theoretically expected quantity of charge was collected. This gave rise to a secondary peak in the distribution below the expected main peak. In bad cases, the secondary peak might be larger than the expected main peak and sometimes be so diffuse as to fill in the distribution below the expected energy loss. Good detectors could be identified in which this effect was small. In principle, such an effect would have a similar effect on the responses of the channels to the geometric path length distribution problem and could be taken into account if properly calibrated. Unfortunately, it was found that the effect in any given detector is unstable with time making calibration of doubtful value.

In spite of these effects, some quite reliable data can be obtained from the detector system by utilizing the basic moderator thresholds and treating the outputs from each channel as effective integral channels. Thus differencing P5 and P6 + P7, taking into account the differing geometric factors gives a differential response from 36 to 80 MeV. P6 + P7 can be regarded as an integral channel for Ep > 80 MeV. Some actual examples of this technique using calibration data are shown in figure 4.16. At lower energies, the channels derived from D3 should be free of the

secondary peaking effect. In satellites beyond the first 3, it is proposed to replace the dome detector assembly with an assembly using planar disc detectors and eliminate some of the problems of the present design.

4.2.3 Accumulators and Telemetry Interface

The level sensor outputs from the Signal Analyzer Unit are logically combined in the Data Processor to form independent outputs of pulses corresponding to events satisfying the requirements of each channel. Two accumulators are provided which are multiplexed between the channels in a compromise sequence designed to optimize the limited telemetry capacity available. Both accumulators are quasi-logarithmic compression counters, one with 7 bit and the other with 8 bit word outputs. The former, reading out in word 53, has a maximum capacity before overflow of 8107_{10} counts and the latter reading out in word 31 and 63, of 44971_{10} counts. The use of a logarithmic compression provides the capacity required to avoid overflow in large events while approximately equalizing the statistical and resolution uncertainties over the mid range of operation. A block diagram of the compression counter is shown in figure 4.11. The 7 bit output in word 53 uses an accumulation time of ≃ 2.5 seconds and is multiplexed to serve the four channels P_6, P_7, α_5, and α_6. The 8 bit output uses an accumulation time of ≃ 1.4 seconds and in word 31 has a multiplex sequence of two channels E_1 and P_1 and in word 63 of the remaining 8 channels P_{2-5} and α_{1-4}. The assignments are intended broadly to match telemetry capability with the expected temporal fluctuations and the operational significance of the channels. Both accumulation times are significantly greater than the period of one satellite evolution (0.6 seconds) and therefore provide integration over the spin cycle. However, since the integration period is not exactly a multiple of the spin period, and if significant anisotropy exists, particularly in the low energy channels from the telescope, some dependence on spin angle phasing may exist and beats may be

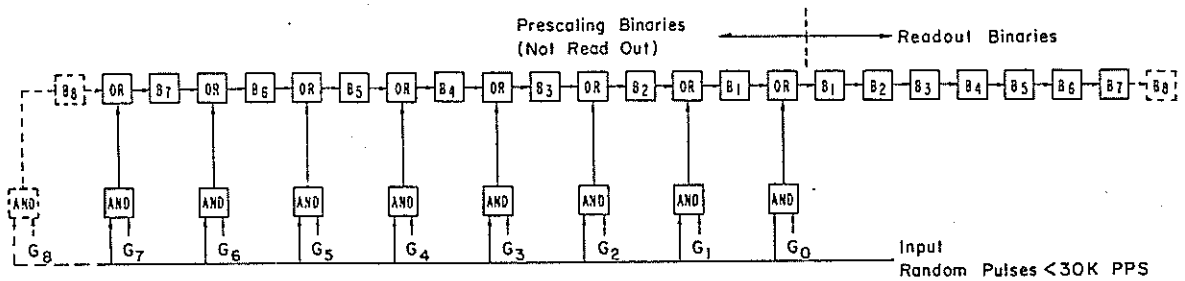

ENABLE	ENABLE LOGIC READOUT BINARY STATES	N READOUT	N INPUT
G_0	$\bar{3}\,\bar{4}\,\bar{5}\,\bar{6}\,\bar{7}\,\bar{8}$	0-3	0-3
G_1	$3\,\bar{4}\,\bar{5}\,\bar{6}\,\bar{7}\,\bar{8}$	4-7	4-11
G_2	$4\,\bar{5}\,\bar{6}\,\bar{7}\,\bar{8}$	8-15	12-43
G_3	$5\,\bar{6}\,\bar{7}\,\bar{8}$	16-31	44-171
G_4	$\bar{5}\,6\,\bar{7}\,\bar{8}$	32-47	172-427
G_5	$5\,6\,\bar{7}\,\bar{8}$	48-63	428-939
G_6	$\bar{5}\,\bar{6}\,7\,\bar{8}$	64-79	940-1963
G_7	$5\,\bar{6}\,7\,\bar{8}$	80-95	1964-4011
G_8	8 OR 6 7 8	96-255	4012-44971

8-Bit Compression Counter

ENABLE	ENABLE LOGIC READOUT BINARY STATES	N READOUT	N INPUT
G_0	$\bar{3}\,\bar{4}\,\bar{5}\,\bar{6}\,\bar{7}$	0-3	0-3
G_1	$3\,\bar{4}\,\bar{5}\,\bar{6}\,\bar{7}$	4-7	4-11
G_2	$4\,\bar{5}\,\bar{6}\,\bar{7}$	8-15	12-43
G_3	$5\,\bar{6}\,\bar{7}$	16-31	44-171
G_4	$\bar{5}\,6\,\bar{7}$	32-47	172-427
G_5	$5\,6\,\bar{7}$	48-63	428-939
G_6	$\bar{5}\,\bar{6}\,7$	64-79	940-1963
G_7	(5 OR 6) AND 7	80-127	1964-8107
G_8	OMITTED		

7-Bit Compression Counter

Figure 4.11 Compression Counter Functional Diagram

observed between the spin and telemetry rates. In principle, this might provide some additional information. The effect can be removed to any desired extent by further averaging in ground data processing.

4.2.4 Electrical Calibration

A calibration system for the pulse electronics is provided which can be exercised under ground command. All preamplifier inputs are simultaneously excited with a 10 kHz pulse rate whose amplitude is modulated with a linear ramp synchronized with the telemetry frame. The peak level of the pulses is changed sequentially over 4 successive groups of 8 frames while changes are made in the channel selection logic to permit all channels to be exercised and the settings of all level sensors checked. However the detectors are not disabled during the sequence so that the calibration is superimposed on the natural background existing at the time. Thus for precise use of the calibrator, it will be necessary to choose a period when the natural environment is most stable and average however many calibration cycles minus background as are required to give the required precision. Table 4.2 summarizes the calibration cycle and also gives the typical channel increments due to the calibrator.

Table 4.2 EPS Calibration Cycle

Frames	Condition	Expected Total Counts (Counts/Sec) Flight A Sensor*														
		E_1	P_1	P_2	P_3	P_4	P_5	P_6	P_7	A_1	A_2	A_3	A_4	A_5	A_6	
1-8	Ramp peak ≈0.7 MeV Level sensor 4 simulated 14336 pulses per ramp		3827 (2665)	3827 (2665)	4139 (2882)	-	-	-	-	-	-	-	-	-	-	
9-16	Ramp peak ≈4.5 MeV Level sensor 2 simulated 14336 pulses per ramp	9638 (6711)	9590 (6678)	10,098 (7032)	640 (446)		10,231 (7125)	7419 (2980)	3957 (1187)		2615					
17-24	Ramp peak ≈19 MeV Level sensor 2 simulated Level sensor $\overline{3}$ inhibited 14336 pulses per ramp	5850 (4074)	2682 (1868)	8836 (6153)		7354 (5121)	13,353 (9299)	12,690** (5092)	708 (284)		11,543 (8038)	2816 (1961)				
25-32	Ramp peak ≈45 MeV No level sensor simulation 14336 pulses per ramp	2700 (1880	1058 (737)	52 (36)		9746 (6787)	10,907 (7595)	8325 (3343)	326 (131)		13,048 (9086)		1371 (955)	2975 (1195)	5248 (2108)	

*Note: The actual number of counts obtained will vary between instruments due to variations in effective ramp peak energy at the individual detectors and variations in exact level sensor settings.

**This counting rate causes the 7-bit counter to overflow leading to a reading of 12680-8107 = 4573 (1836).

4.3 Nuclear Calibration

Calibrations of the counting efficiency versus energy have been carried out for both the telescope and dome detectors and their associated electronics over much of their range. Calibration of the flight telescope channels axial response was carried out at the Stanford University Linac with protons in the range from ≈ 2-15 MeV and alphas from 4 to 24 MeV. In addition, some data were taken off axis for the engineering model telescope.

Calibration of the flight dome assemblies for normal incidence was carried out at the Harvard Cyclotron facility for protons in the range of approximately 25-145 MeV. Typical results from these calibrations are shown in figures 4.12, 4.13, and 4.14. A summary of the detector properties and level sensor settings for the three instruments is shown in tables 4.3 and 4.4. Complete details are available in a summary of the calibration methods and data (Reference 4.3). Because of the special uncertainties associated with the dome calibration, the flight B dome was subjected to a particularly thorough calibration at a sufficient number of incident angles to be able to estimate the true omnidirectional response. The methods and results are described in Reference 4.3 and 4.4. Figure 4.15 shows the omnidirectional response obtained. Figure 4.16 shows the result of using the detector outputs to derive responses depending as far as possible only on the moderators for high energy discriminations and affected as little as possible by instabilities in the detector response.

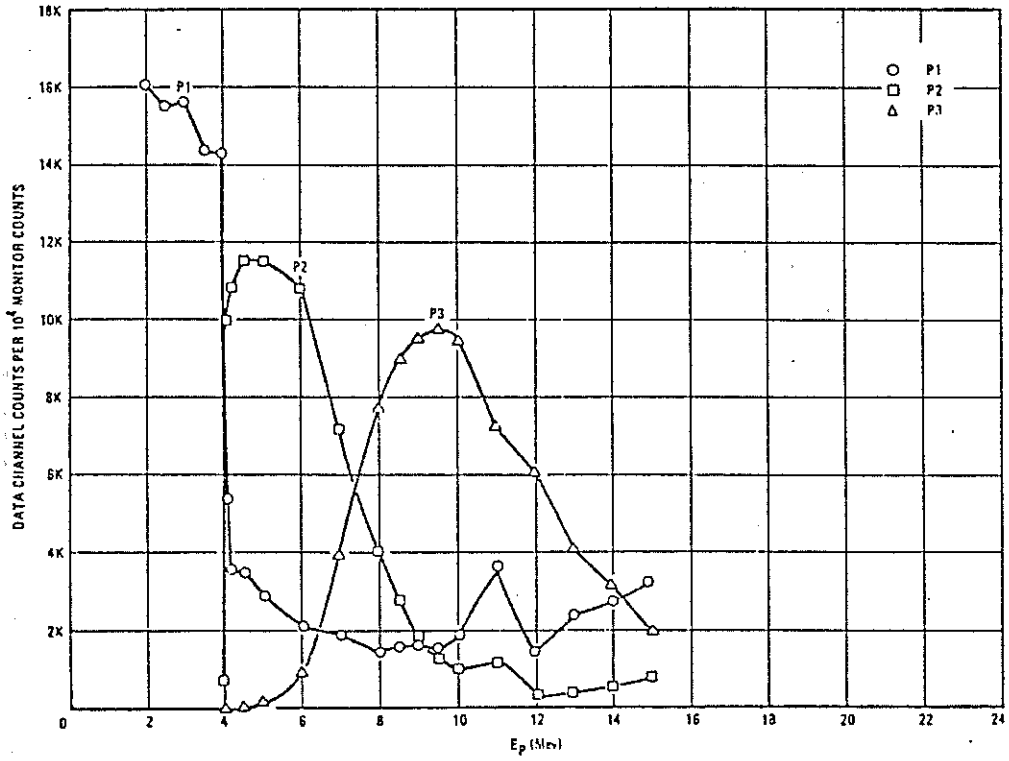

Figure 4.12 Flight "C" Unit, 7/2/73, Stanford University, M. Rinehart, A. Ramos, Runs 44-66, Book 22905, p. 16

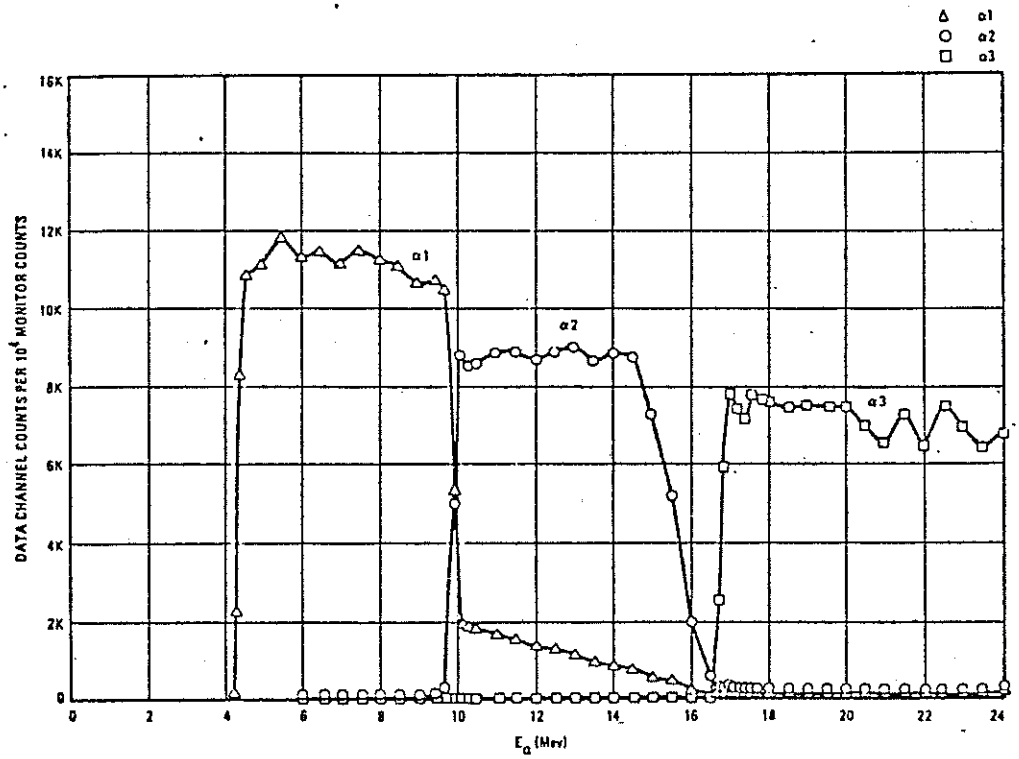

Figure 4.13 Flight "B" Unit, 7/9/73, Stanford University, H. Brown, F. Currlin, Runs 96-149, Book 22905, pp. 23-25

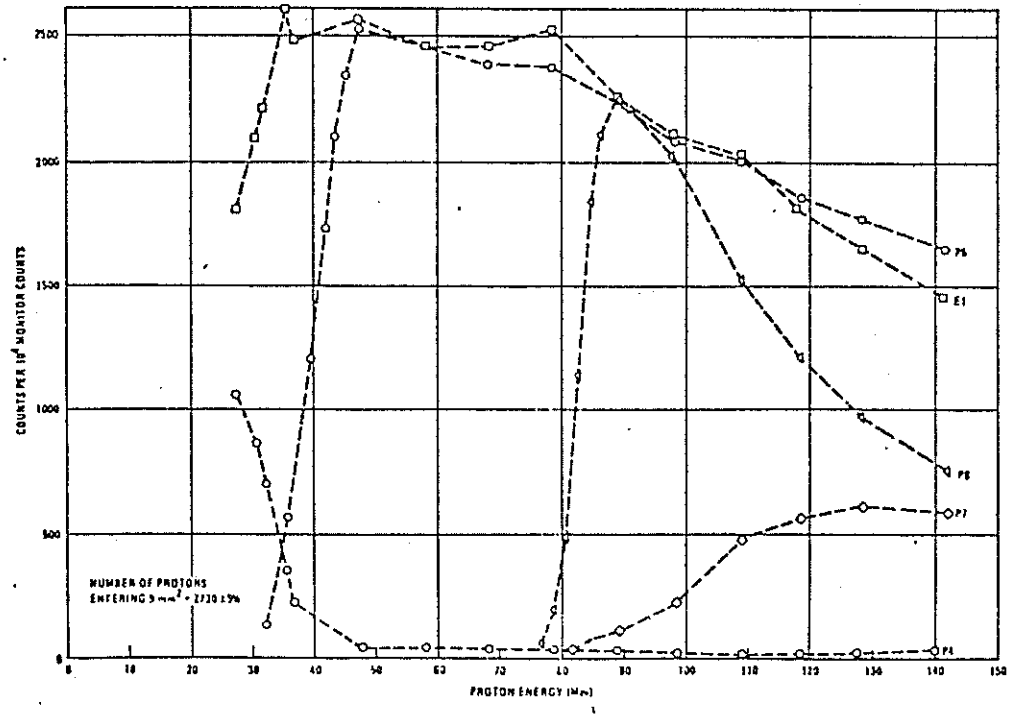

Figure 4.14 "C" Dome Calibration, Harvard University, 8/15/73, F. Currlin, M. Rinehart, Book 25394, pp. 7-10

Table 4.3 Telescope Configurations

Parameter		Assembly		
		Protoflight A	Flight B	Flight C
D1	Serial #	11-483E	11-456J	11-456C
	Thickness (min)	48.8 ± 1 μ	48.1 ± 1 μ	49.5 ± 1 μ
	Area (nominal)	100 mm^2	100 mm^2	100 mm^2
	LS 1 threshold	0.30 Mev	.33 Mev	.32 Mev
	LS 2 "	0.52 Mev	.50 Mev	.50 Mev
	LS 3 "	3.5 Mev	3.5 Mev	3.7 Mev
D2	Serial #	11-494D	11-244J	12-173C
	Thickness (min)	499 μ	512 μ	495 μ
	Area (nominal)	100 mm^2	100 mm^2	100 mm^2
	LS 4 threshold	3.3 Mev	3.8 Mev	3.8 Mev
	LS 5 "	14.0 Mev	13.9 Mev	16.0 Mev

Data Channel	P1	P2	P3	α1	α2	α3
LS Logic	$2\,\bar{3}\,\bar{4}$	$2\,\bar{3}\,4\,\bar{5}$	$1\,\bar{2}\,4\,\bar{5}$	$3\,\bar{4}$	$3\,4$	$2\,\bar{3}\,5$

Table 4.4 Dome Configurations

Parameter		Assembly		
		Protoflight A	Flight B	Flight C
D3	Serial #	003	006	020
	Thickness	2.74 mm	2.77 mm	2.64 mm
	LS 6 threshold	1.74 Mev	1.57 Mev	1.64 Mev
	LS 7 "	10.8 Mev	10.1 Mev	10.63 Mev
	LS 8 "	43.5 Mev	37.2 Mev	42.7 Mev
D4	Serial #	021	039	005
	Thickness	2.67 mm	2.79 mm	2.80 mm
	LS 9 threshold	1.34 Mev	1.58 Mev	1.48 Mev
	LS 10 "	33.6 Mev	33.5 Mev	30.5 Mev
D5	Serial #	007	002	042
	Thickness	2.76 mm	~1.5 mm	2.76 mm
	LS 11 threshold	1.58 Mev	1.91 Mev	1.84 Mev
	LS 12 "	2.75 Mev	2.88 Mev	2.68 Mev
	LS 13 "	32.9 Mev	35.1 Mev	31.9 Mev

Detector	D3			D4		D5		
Data Channel	E1	P4	α 4	P5	α 5	P6	P7	α 6
LS Logic	$6\,\bar{7}$	$7\,\bar{8}$	8	$9\,\bar{10}$	10	$12\,\bar{13}$	$11\,\bar{12}$	13

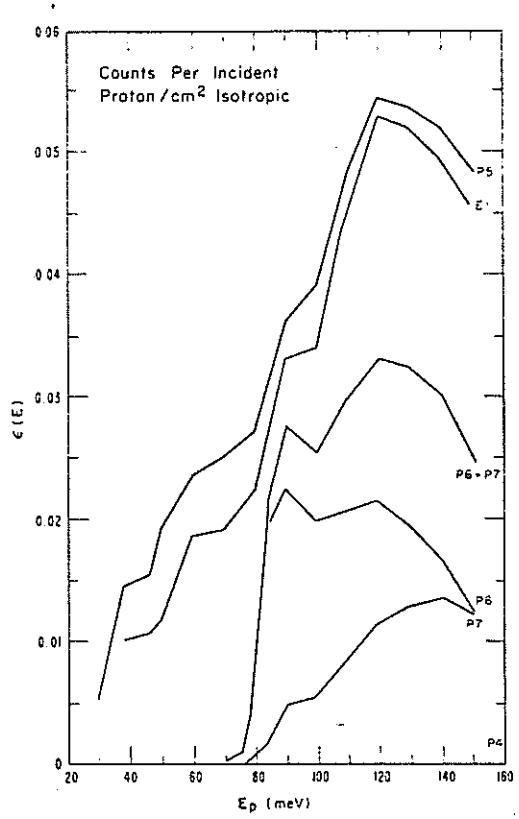

Figure 4.15 Omnidirectional Proton Response

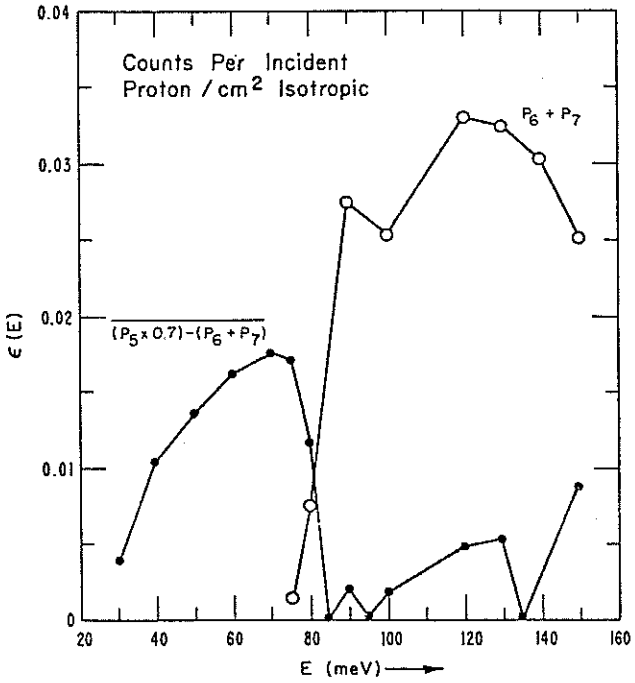

Figure 4.16 Differencing of Omnidirectional Responses

5. THE MAGNETOMETER

5.1 Requirements

The objective of the magnetometer is to permit monitoring of the strength and direction of the magnetic field at the satellite. With two or more satellites at different local times, the data should permit routine modeling of the geomagnetic field as modified by the varying solar wind and other effects.

The SMS has not been constructed as a "clean" magnetic spacecraft and will, therefore, produce interfering fields which will be superimposed on the measurement of the earth's field. As in the earlier ATS-1 and ATS-5 satellites, it is expected to be possible to subtract these effects with some confidence using ground calibrations and actual experience of the effects of the spacecraft in its various operating modes.

The requirements for and the design of the SMS magnetometer are patterned on the successful instrument on the ATS-1 spacecraft which is a similar spin stabilized vehicle (Reference 5.1). The basic requirements which were set for the instrument are shown in table 5.1. The SMS instrument has a considerably more sophisticated onboard signal processing system than the ATS-1 instrument in order to accommodate a greatly reduced telemetry capability and ease the ground based processing requirements.

Table 5.1 Magnetometer Performance Characteristics

FIELD VARIABLE	DATA CHANNEL/RANGE	ERROR SOURCE/MAGNITUDE LIMIT	DATA SAMPLING RATE/PASSBAND
PARALLEL COMPONENT MAGNITUDE	ANALOG "FINE" LINEAR 0-5 V ±50γ	DIFFERENTIAL LINEARITY 0.2γ INTEGRAL LINEARITY 0.5γ ZERO OFFSET VS TIME 3.5γ VS TEMP. 1.0γ VS BUS 0.2γ NOISE 0.1γ	1.35 SAMPLES/SEC DC - 0.25 HZ
	DIGITAL, "COARSE" -1120 TO +1400γ	LARGER OF 0.5% OR 0.5γ	0.34 SAMPLES/SEC
TRANSVERSE COMPONENT MAGNITUDE	ANALOG LINEAR 0-5 V SELECTABLE FULL SCALE	DIFFERENTIAL LINEARITY 10 mV INTEGRAL LINEARITY 25 mV ZERO OFFSET VS TIME 20 mV VS TEMP. 20 mV VS BUS 10 mV NOISE 5 mV (P-P) RIPPLE 0.1% (P-P) DC RESPONSE 20 mV	1.35 SAMPLES/SEC DC - 0.25 HZ
	DIGITAL, FULL SCALE ±50, 100, 200, 400γ	0.5%	0.34 SAMPLES/SEC
VECTOR DIRECTION	DERIVED FROM MAGNITUDES	MAGNITUDE ERRORS TRANSVERSE PHASE AT AMBIENT 0.5° VS TEMP. 1.0° VS SPIN RATE 3° PER R/MIN	N/A

5.2 Instrument Design

5.2.1 Sensors

The basic sensor used in the ATS-1, -5, and the SMS instrument is the flux gate. It has been shown to be very reliable in space and is well suited to the measurement of fields in the 50-200 γ region anticipated in geostationary orbit. The combined effects of temperature coefficients and zero offsets can be held to 1 γ or less. The operation of a flux gate sensor is shown in figure 5.1. A magnetic core with a rectangular hysteresis characteristic is driven alternately into saturation in opposite directions by a symmetrical drive signal from an oscillator. In the absence of any external field, the flux waveform would be perfectly symmetrical and, therefore, contain no even harmonics. If an external bias field is present, the switching points will become assymmetrical causing the flux waveform to contain second and higher even order harmonics which can be used as a measure of the external field. To facilitate the measurement of the small harmonic components, the sensor is usually arranged so that the drive MMF is applied to two sections of the core arranged as a complete magnetic circuit so that the external flux at the drive frequency is very small. A second pair of windings connected in antiphase and thus balancing the fundamental then has in phase second harmonics due to an external field which is itself effectively in opposite directions in the two halves. Because of the effects of temperature on the core material, the basic sensor is normally only used as a null detector. A third coil encompassing the whole core assembly is used to complete a high gain feedback loop from the output of a tuned amplifier and coherent detector system at the second harmonic frequency thus forcing the core flux to zero and the coil current to be accurately proportional to the external field.

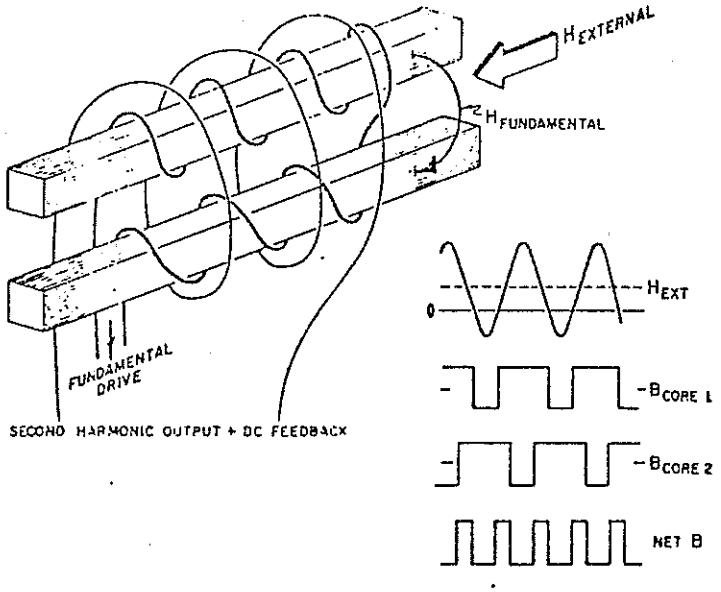

Figure 5.1 Basic Flux Gate Sensor

5.2.2 Sensor Configuration

There are a number of possible ways of arranging single axis sensors on a spinning satellite to give a vector field measurement. A single sensor can be set at ≈55° to the spin axis and will then scan through three orthogonal axis symmetric with respect to the spin axis. Alternatively two sensors may be employed, one parallel to the spin axis and the second transverse to it. A varient of this configuration used in the ATS-1 instrument is an orthogonal pair arranged symmetrically with respect to the spin axis and in the plane containing it. Signals equivalent to the parallel and transverse axis can then be obtained by sum and differencing the outputs. The configuration chosen for the SMS/GOES satellite is that of the simple parallel and transverse sensor. This provides for simpler signal processing and some degree of protection against single point failure compared with the single sensor scheme in that the number of failures causing loss of all three axes is reduced. The sensors are aligned parallel and transverse to the spin axis rather than in the alternate configuration as it did not seem practical to gain any advantage by this means in case of a sensor failure unless the signal processing electronics, which are significantly different for the two axes, were duplicated. In the absence of vehicle interfering fields, the parallel sensor output is directly a measure of the external field along the spin axis and the output of the transverse sensor is a spin frequency sinusoid whose amplitude and phase are measures of the strength and direction of the transverse field.

5.2.3 Dynamic Range Requirements

The range of natural fields likely to be encountered in geostationary orbit at 6.6 R_e is relatively small encompassing 100-200 γ on the parallel axis and a few tens of γ in the transverse with perhaps twice these values under disturbed conditions. However, the spacecraft, not being magnetically controlled, may introduce large static and dynamic offsets. Based on previous experience with the ATS-1 instrument, the specification was, therefore, imposed that the instrument must simultaneously accommodate natural fields of ± 400 gamma and spacecraft fields of ± 800 γ. This is achieved on the parallel axis by a stepping offset field generator giving a range of 64 steps of 40 γ in conjunction with a basic instrument range of ± 50 γ. The offset generator is automatically triggered when the basic output approaches either full scale value. The total range covered is from +1450 to -1170 γ, the center offset being chosen to allow equal margin for the expected field of +150 γ when the spacecraft axis is in the normal direction. At the other end of the scale, the 9 bit telemetry provides a basic resolution of 0.2 γ in the ±50 γ range and the basic instrument noise level, which is the determining factor in the analysis of the data by power spectral density, is specified as ≤ 0.1 γ peak-to-peak.

The use of a stepped offset technique is not particularly practical in the transverse channel, nor is it really required since the large components of the spacecraft field are likely to be static or quasi-static and are removed by the DC feedback in the basic sensor. The required more

limited dynamic range to cover the natural environment and possible spacecraft spin fundamental fields is provided by autoranging with 4 sensitivites, ±50, ±100, ±200, and ±400 γ. Thus providing the spacecraft fields are reasonably small, the same ±50 γ sensitivity and resolution is available on all axes. If the instrument is upranged by the natural field, then the percentage resolution will be maintained at a reasonable value.

5.2.4 Signal Processing

The telemetry capacity (≈ 64 bps) allocated to the total SEM precludes the direct transmission of the output of spin frequency signals (1.6 Hz) to the ground. Signal processing must, therefore, be carried out on the satellite to provide band limited signals representing the vector field and compatible with the telemetry sampling rate.

An important requirement that the signal processing system must meet is that it should not degrade the ability to separate onboard interfering fields from those of natural origin. The interfering fields can be divided into two classes for each axis, those which a priori cannot be distinguished from natural fields and those which can be. In the first class are:

1. For the parallel axis, static spacecraft fields arising from permanent magnetism of the structure and components and from the DC component of currents flowing in the spacecraft systems.

2. For the transverse axis, spacecraft fields arising from currents having spin frequency fundamental components such as those generated by portions of the solar array and systems carrying spin related signals such as the ADAC and communication subsystems.

In the second class are:

3. For the parallel axis, all spin frequency fundamental and harmonic components, particularly if these could be aliased by the telemetry sampling rate into the frequency range of the instrument.

4. For the transverse axis, spacecraft static fields and spin harmonic frequency fields, since these cannot be generated from external fields.

A very much simplified block diagram of the instrument in figure 5.2 shows how the signal processing is arranged to provide outputs compatible with the telemetry limitation.

In the transverse axis, overall feedback is applied via an integrator stage to null the static component of the field seen by the sensor.

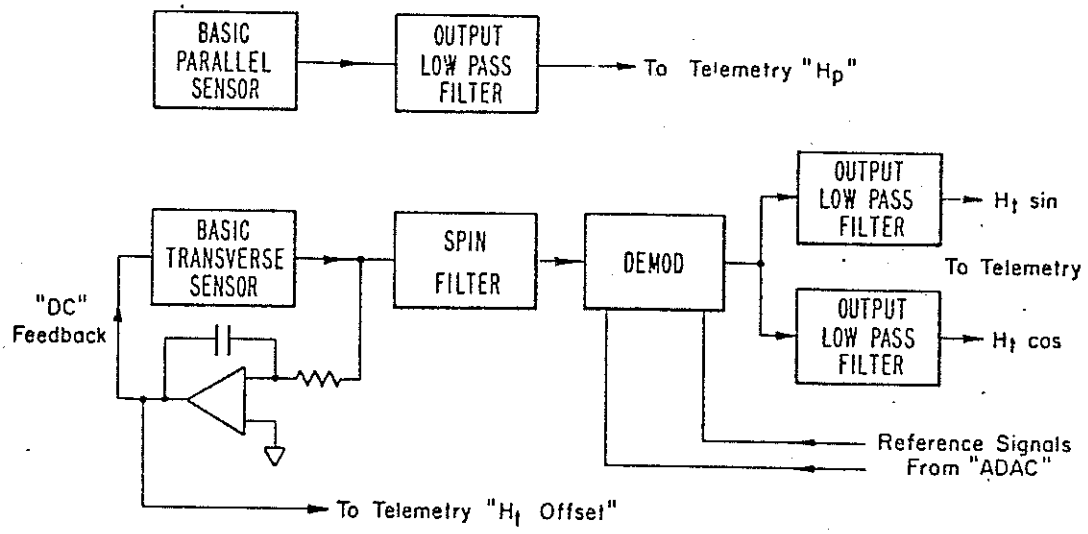

Figure 5.2 Magnetometer Signal Processing

The signal from the sensor is then passed through a filter designed to pass the 1.67 Hz spin frequency but attenuate the third and higher order harmonics by >35 dB. The filtered signal is then applied to a pair of balanced synchronous demodulators driven in quadrature by square wave signals derived from the spacecraft ADAC subsystem. These produce two bipolar voltages representing the X and Y components specifying the field vector having an amplitude and direction angle in a coordinate system set by the timing of the reference signals and the delays in the predemodulator electronics. The bandwidth of the signals prior to sampling by the telemetry system is set by the pair of low pass filters.

In the parallel axis, the output of the basic sensor is used directly after passing through the output low pass filter to restrict the bandwidth prior to sampling.

To accommodate as much as possible of the geomagnetic spectrum of interest, the three data outputs, referred to as H_p, $H_t \sin$ and $H_t \cos$ are sampled on a supercommutated basis with four samples per main frame of telemetry, or a sampling rate of 1.3 per second. This gives a data folding frequency of 0.65 Hz. The geomagnetic field spectrum drops off in energy at least proportional to $1/f$ and possibly $1/f^2$ in this part of the spectrum. However, the spacecraft noise will be significant at the 1.6 Hz spin frequency and its harmonics and the transverse channel demodulator outputs contain large components at the spin frequency second harmonic. These signals will, therefore, be the most significant when considering protection against aliasing in the sampling process. In view of the unknown magnitude of much of the spacecraft noise at the time that

a decision had to be taken on the low pass filter characteristics, a conservative approach was adopted. The filters selected are of a 3 pole Butterworth type which provides a maximally flat amplitude response and a well damped transient response. A -3 dB cutoff frequency of 0.136 Hz was selected to provide a minimum of 40 dB of protection at the folding frequency and > 70 dB protection against the spin frequency and its harmonics. More complex filters with sharper cutoff performance were rejected as likely to degrade the instrument stability and reliability. At least some of the advantages of a more complex filter can be achieved by ground processing to unfold the instrument filter response although, depending on the amplitude of the signals being unfolded, this process will be limited eventually by the telemetry quantization noise (0.2γ). Another consideration affecting the filters is the requirement to be able to remove the transients generated by the automatic changes in offset and range. To do this easily, not only must the transient response of the instrument, determined primarily by the output filters, be known, but the timing of the transient should also be known. As far as the filters are concerned, this has been facilitated as much as possible by imposing requirements for close matching between the filters. The timing requirement is met in the majority of cases by the arrangement of the range and offset logic which is described in more detail in section 5.2.6.

5.2.5 Calibration

Overall calibration of the sensor involves both a knowledge of the sensor response and of the offsets introduced by the spacecraft. As previously stated, the SMS spacecraft is not a magnetically clean spacecraft, and the offsets from it must be considered very seriously. Ground calibrations of the spacecraft permanent field and of the stray fields from the onboard electrical systems have been made (Reference 5.2). However, these can only be regarded as approximate as the "permanent" field may well change between calibration and the final orbital state, and some onboard systems, such as the solar panels, are extremely difficult to operate realistically under simulation conditions. Thus the final values for offsets must be determined after the spacecraft is in orbit either by observation of the data or comparison of the data with that from other spacecraft. It is possible that sometime during the life of the spacecraft, the spin axis will be inverted for operational reasons connected with the VISSR cooler. If this is done under quiet magnetic conditions, then an excellent offset calibration of the H_p axis should be obtained.

The calibration of the sensors themselves is expected to be very stable because of the feedback field nulling nature of their operation. Flux tank calibrations have been made and these basic calibrations are given in reference 3.8. However to verify the correct operation and compensate for any gain changes in the overall signal processing and telemetry channel an In Flight Calibrator (IFC) is included. The IFC is initiated by a command to the magnetometer and, after the 144 main frame sequence is complete, the calibration terminates automatically. Table 5.2 shows the sequence for the two axes. On the parallel axis, currents

Table 5.2 Magnetometer Calibrate/Data

Zero: Normal Data Mode
One: Calibrate Mode

1 - Sequence

a) Magnetometer calibrate start command 044 execute received.

b) on the next Main Frame Start pulse from the telemetry generator, the calibrate cycle starts, indicated by the Magnetometer Calibrate/Data bit rising to the "1" state.

c) for TM frames 0-15 subsequent to (b) above the instrument continues to monitor natural and satellite magnetic field intensities as in the "Data" mode.

d) for TM frames 16 - 143 calibration signals are added to the natural and satellite magnetic fields in accordance with the table below:

	Gamma Calibrate Levels		Relative Phase Degrees
	H_p	H_t	H_t
16-31	+25	25	90
32-47	-25	25	0
48-63	+250	25	270
64-79	-250	25	180
80-95	+25	250	90
96-111	-25	250	0
112-127	+250	250	270
128-143	-250	250	180

e) at the receipt of the 144th Main Frame Start pulse from TM, the instrument automatically reverts to the data mode as indicated by the calibrate/data bit dropping to the "0" state; however, three subsequent Main Frame Start pulses are required to assure return of the H_t range and Hp offset to nominal condition.

are applied to the calibration coil on the sensor corresponding to fields of $\pm 25\ \gamma$ and $\pm 250\ \gamma$. On the transverse axis, the reference square waves supplied by the ADAC subsystem are used to generate current square waves which correspond to external field intensities of the same magnitudes, +25 and $\pm 250\ \gamma$, at four angles, 0, 90, 180, and 270° obtained by selection of the appropriate reference signal or its complement. This calibrates both the amplitude response and the phase response of the transverse channel. The calibration fields are added to the natural fields present at the time of the calibration.

5.2.6 Overall Operation

A complete block diagram of the instrument is shown in figure 5.3. The general mode of operation should be apparent from this and from the foregoing descriptions of parts of the system. The overall operation of the automatic offset and range changing will be described here. A photograph of the magnetometer instrument is shown in figure 5.4.

In the parallel axis, the output from the H_p sensor electronics is first filtered by a low pass filter with a 3 dB frequency of 2.5 Hz before being applied to the level sensors and logic in the H_p offset field generator. The purpose of this filter is to reduce the difference between

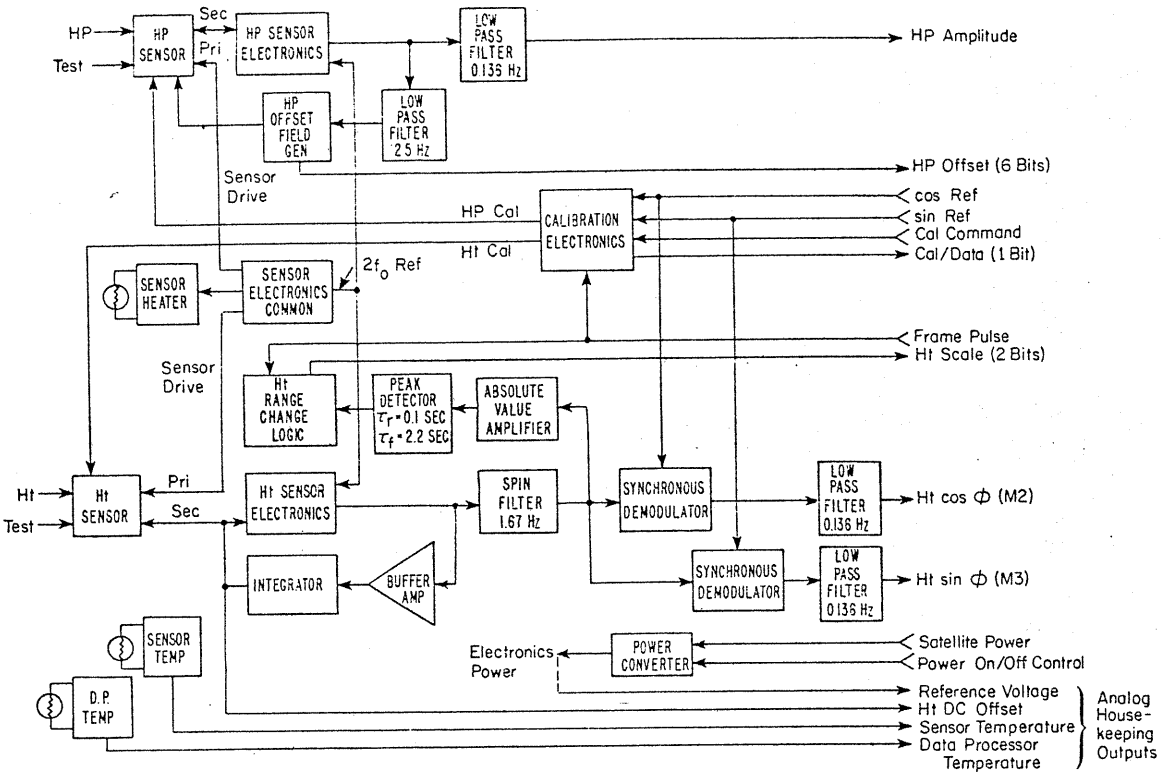

Figure 5.3 SMS Magnetometer Block Diagram

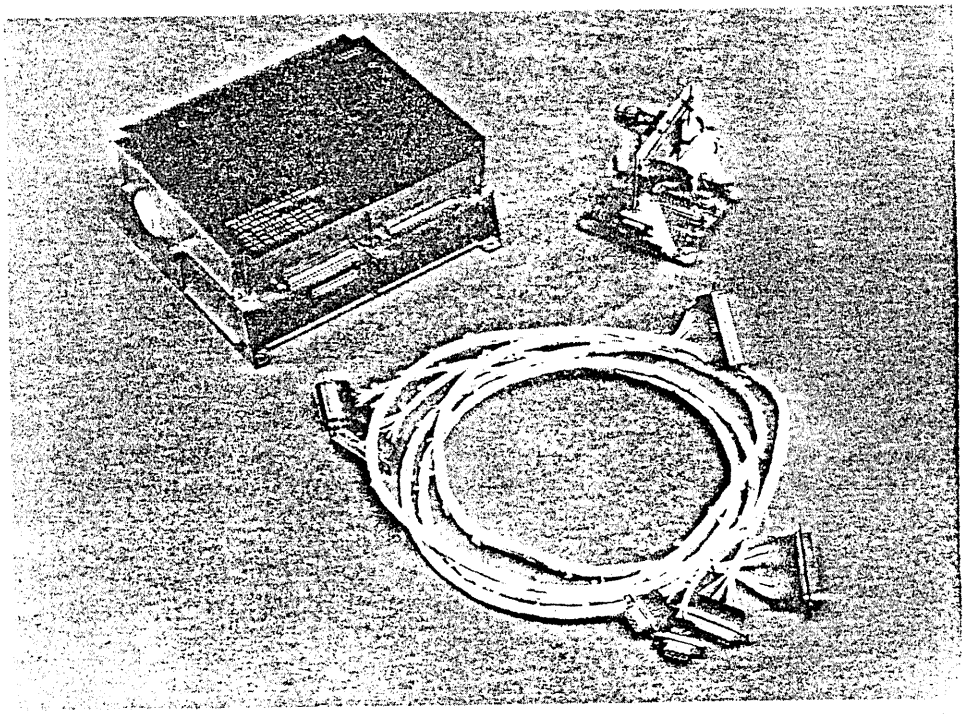

Figure 5.4 Magnetometer System

the sensor bandwidth of approximately 100 Hz and the final output bandwidth of 0.136 Hz so that transient fields which might be generated by the spacecraft do not unnecessarily initiate offset changes. The bandwidth is a compromise between equalizing the noise bandwidth and limiting the slew rate of the channel to rapidly changing inputs. When the output of the H_p sensor approaches $\pm 50\ \gamma$, an offset step of 40γ in the appropriate direction is introduced. When analyzing the data from slowly changing inputs, it would be very desirable to be able to accurately remove the transient generated by an offset step change. To do this, in general, requires a knowledge of the instrument transient response and a knowledge of the time the transient occurred. To simplify this reconstruction, the H_p offset generator is inhibited from initiating a step until the occurrence of the start of a main frame. This not only fixes the timing but enables the H_p offset reading, which occurs twice per main frame to be unambiguously read. Again there is a compromise between ideal performance for slowly varying inputs and the slew rate of the system when subjected to a step change in input. To prevent the slew rate becoming unacceptably low under the latter condition, which occurs in the cal cycle, and may also occur naturally during the passage of a shock disturbance or passage through the magnetopause under unusual compression, the offset generator is allowed to continue stepping, once initiated at a rate determined by an internal timing generator set to 4 Hz. Thus a maximum of 12 steps can be made per frame, or 4 steps per second permitting readjustment to a step at a rate of 160γ per second. Under these conditions, reconstruction of the input step is, of course, impossible because of the basic bandwidth limitation in the telemetry channel. However, the important consideration then is that the instrument itself should follow sufficiently quickly that it does not become the basic limitation.

In the transverse channel, similar considerations apply. Here the bandwidth limitation at the input to the range change logic is supplied by the bandwidth of the spin filter. A fast charge slow discharge peak detector is employed to provide a more suitable input to the level detector than the absolute value of the spin component. Again, similarly to the parallel channel, the logic is constrained to make changes coincident with the start of a main frame. With the limited number of ranges, no provision is made for more than one step per frame. Figure 5.5 shows the range change timing and filter responses in more detail.

Power for the experiment is provided by a standard DC/DC convertor. Analog housekeeping provides a reference voltage, the H_t sensor DC offset, the sensor and the electronics package temperatures.

5.2.7 Calculation of the Vector Field

The constants used here refer to the SMS-A instrument and may require minor correction for the later satellites. H_p fine is calculated from

$$H_p \text{ fine} = -20.06\ (X - 2.455),$$

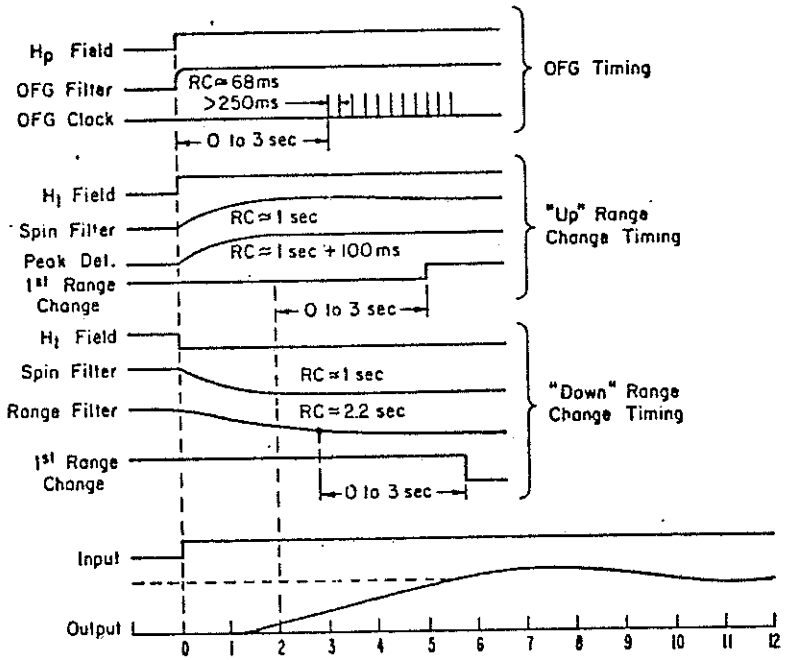

Figure 5.5 Magnetometer Response (Seconds)

where X is the voltage (0-5.12 V) represented by either word 6, 22, 38, or 54. H_p step is calculated from

$$H_p \text{ step} = -40\ (H_p \text{ offset} - 28)$$

where HP offset is the decimal number given by the most significant six bits of either word 5 or word 36. H_p is then

$$H_p = H_p \text{ fine} + H_p \text{ step}.$$

The inversions in H_p fine and H_p step are included to obtain the + z component of magnetic field, since the magnetometer output is positive for fields along the - z axis.

H_t is calculated from

$$H_t = K \sqrt{(H_t \sin \phi - 2.5)^2 + (H_t \cos \phi - 2.5)^2},$$

where

$$K = 20(2^i)$$

H_t sin = voltage represented by word 8, 24, 40, or 56

H_t cos = voltage represented by word 7, 23, 39, or 55

i = scale of 0, 1, 2, or 3 depending on bits 7 and 8 of word 5 or 36.

The angle PHI is the angle in the spin plane between the projections of the satellite to earth line and the magnetic field, measured from the earth to the field, counter clockwise when observed from positive z. The raw data must be corrected for the angle of the magnetometer H_t axis away from the spacecraft y axis (52° 33' on SMS-A) and the electronic phase shift within the magnetometer which varies with range. Thus,

$$PHI = Tan^{-1}\left(\frac{H_t \sin \phi - 2.5}{H_t \cos \phi - 2.5}\right) + \theta$$

where θ is given as a function of range by the following table. (Actual instrument values for the electrical phase shift may be obtained from the IFC data.)

Range	θ
0	-76.2°
1	-80.4°
2	-82.5°
3	-83.6°

Note that PHI is measured in despun body coordinates. Thus the sense of PHI and H_p in earth-based coordinates will be reversed between the normal and inverted spacecraft configurations. Despun body coordinates are defined as a coordinate system with the z axis along the spacecraft z axis, the y axis in the spin plane such that the y-z plane contains the satellite to earth vector, and x completing a right-handed system.

ACKNOWLEDGMENT

The total team with responsibility including the SMS SEM encompasses nearly the whole NASA, GSFC; NOAA/NESS/ERL; and the WDL Division of Aeronutronic Ford Corporation* SMS project staff. Particular thanks for their support are due to Mr. Don Fordyce, SMS Program Manager at GSFC, and Dr. D. J. Williams of the Sciences Directorate of GSFC and latterly Director of the Space Environment Laboratory.

Those primarily concerned with the detailed design of the SEM were:

Mr. Herb Brown, Aeronutronic Ford* SMS Project

Dr. Richard Donnelly, NOAA, ERL

Dr. Harry Farthing, GSFC

Mr. Richard Grubb, NOAA, ERL

Mr. Don McMorrow, Aeronutronic Ford* SMS Project

Mr. W. Nicolls, Keithley Electronics

Dr. Marion Rinehart, Aeronutronic Ford SMS Project

Mr. Terry Sheridan, Keithley Electronics

Mr. Tom Skillman, GSFC

Mr. George Takahashi, Aeronutronic Ford* SMS Project

Dr. A. M. Young, Aeronutronic Ford* SMS Project

Much valuable help and advice in the early planning and in reviewing problem areas were provided by:

Dr. C. Bostrom, Applied Physics Laboratory

Dr. W. Campbell (then) NOAA, ERL

Dr. Paul Coleman, UCLA

Mr. R. W. Kreplin, Naval Research Laboratory

Dr. S. Krimigis, Applied Physics Laboratory

Dr. G. Paulakis, Aerospace Corporation

Dr. G. Reid, NOAA, ERL

Dr. H. Sauer, NOAA, ERL

Mr. Robert Snare, UCLA

*Formerly Philco-Ford Corporation

6. REFERENCES

3.1 Wende, C. D. (1971), The Normalization of Solar X Ray Data from Many Experiments, GSFC Report X60177-166.

3.2 Grubb, R. N. (1969), The Design of an X Ray Sensor for the GOES Space Environment Monitor (SEM), unpublished SEL report.

3.3 Paulikas, G. A., J. B. Blake, J. A. Palmer (1969), Energetic Electrons at the Synchronous Altitude: A Compilation of Data, Aerospace Corp. Rept. TR-0066 (5260)-20-4, available in Microfische (AD 864417), National Technical Information Service, Springfield, Va. 22151.

3.4 Vette, J. L., and A. B. Lucero (1967), Models of the Trapped Radiation Environment, Electrons at Synchronous Altitude, NASA Rept. SP3024, Vol. 3.

3.5 Rinehart, M. C. (1970), Evaluation of the Keithley Instrument Co. X Ray Counter Design, Philco-Ford Corp. WDL Rept. IW50SMS-SEM-005.

3.6 Young, A. M. (1972), SMS Sensor Electron Response, Philco-Ford Corp., WDL Rept. 1W50-31.

3.7 Grubb, R. N. (1971), Computer Simulation of SMS X Ray Background Subtraction Signal Processing Techniques, unpublished SEL report.

3.8 Wirth, R. J. (1973), Geostationary Operational Environmental Satellite (GOES)/Synchronous Meteorological Satellite (SMS) Operational Manual, NASA GSFC Report, unnumbered.

3.9 Unzicker, A., and R. F. Donnelly (1972), Calibration of X Ray Ion Chambers for the Space Environment Monitoring System, NOAA TR ERL 310-SEL 31.

4.1 Foelsche, T. (1971), Radiation Measurements and Doses at SST Altitudes, Nat. Symp. on Natur. and Man-Made Radiation in Space, Las Vegas, Nevada.

4.2 Paulikas, G. A. (1968), ATS-1 Omnidirectional Spectrometer, Final Report, Aerospace Corp. Rept. TR0158 (3260-20)-7.

4.3 Rinehart, M. C. (1974), SMS A, B, C EPS Calibration, Philco-Ford Corp. WDL Rept. SMS-PCC-6252.

4.4 Rinehart, M. C. (1974), Recalibration of SMS-B Dome, Philco-Ford Corp. Rept. 3G4600-74-082.

5.1 Barry, J. D., and R. C. Snare (1966), A Flux Gate Magnetometer for the Applications Technology Satellite, IEEE Trans. Nuc. Sci., NS13.

5.2 Contractor Reports, available from the Space Environment Laboratory, Environmental Research Laboratories, National Oceanic and Atmospheric Administration, Boulder, Colorado 80302.